Study of Autophagy in Higher Plant

~ through the analysis of *AtAPG* genes ~

Hideki Hanaoka

Department of Molecular Biomechanics

Graduate Program in School of Life Science

The Graduate School for Advanced Studies

Table of Contents

Abbreviations

AB = autophagic body

AP = autophagosome

API = aminopeptidase I

DTT = dithiothreitol

EDTA = ethylenediamine tetraacetic acid

ER = endoplasmic reticulum

E64c = (2S, 3S)-trans-epocysuccinyl-L-leucylamido-3-methyl-butane

E64d = (2S, 3S)-trans-epocysuccinyl-L-leucylamido-3-methyl-butane ethyl ester

HA = hemagglutinin

mAPI = mature form of API

MS = Murashige and Skoog

ORF = open reading frame

PAGE = polyacrylamide gel electrophoresis

PCR = polymerase chain reaction

PI3-kinase = phosphatidylinositol 3-kinase

PMSF = phenylmethylsulfonylfluoride

prAPI = precursor form of API

RT = reverse transcription

Rubisco = ribulose 1,5-bisphosphate carboxylase/oxygenase

SDS = sodium dodecyl sulfate

TCA = trichloroacetic acid

Summary

Autophagy is an intracellular process for vacuolar bulk degradation of cytoplasmic components. Autophagy is a ubiquitous eukaryotic process and recently, the molecular machinery responsible for yeast and mammalian autophagy has begun to be elucidated at the cellular level. However, the role that autophagy plays at the organismal level are yet to be determined. Therefore, I aimed to study the significance of autophagy in plant for the plant life cycle.

A genome wide homology search revealed significant conservation between yeast and plant autophagy genes. Twenty-five novel plant genes (*AtAPG* genes) were discovered, which are homologous to 12 yeast *APG* genes that are essential for autophagy. Both the functional domains and the amino acid residues essential for yeast autophagy are well conserved in the corresponding AtAPG proteins, suggesting that the Apg system functions in a similar manner in plants as it does in yeast and mammalian cells.

Next, I searched for *AtAPG* knockout plants in T-DNA insertion lines and identified an *Arabidopsis thaliana* mutant carrying a T-DNA insertion within *AtAPG9,* which is the only homologue of yeast Apg9 in Arabidopsis (*atapg9-1*). AtAPG9 was predicted to be a transmembrane protein, and reasonably AtAPG9-GFP showed the fluorescence of dots dispersed throughout the cytoplasm. *AtAPG9* was expressed in every wild-type organ tested, and not in the *atapg9-1* mutant plants.

In the Arabidopsis suspension-cultured cells and root cells that during sucrose starvation, addition of protease inhibitor induced the accumulation of spherical bodies. These spherical bodies were stained with acidtropic dyes quinacrine or neutral red, this phenomena is quite similar to autophagy reported in tobacco suspension cells. This accumulation of spherical bodies was reduced in *atapg9-1,* suggesting that autophagy was defected in *atapg9-1*.

Next, I observed the phenotypes brought about by the null mutation of *AtAPG9* gene. The following phenotypes were complemented by expression of wild-type AtAPG9 gene, confirming that AtAPG9 is responsible for them. Under nitrogen starvation conditions, rapid chlorosis was observed in *atapg9-1* cotyledons and rosette leaves. Under carbon starvation conditions, *atapg9-1* also exhibited rapid chlorosis of cotyledons. Hence, in the nutrient limited condition, autophagy is crucial for retarding chlorosis. Furthermore, *atapg9-1* exhibited a reduction in seed sets when nitrogen supply was limited, suggesting that AtAPG9 is required for efficient nutrient

relocalization in as a whole plant.

In detached leaves, nutrient supply to leaves was cut off and senescence was induced artificially. Detached leaves of *atapg9-1* showed accelerated senescence. Microscopic analysis indicated that there was a reduction in the number of chloroplasts in the epidermal side of wild-type leaf mesophyll cells during senescence. Though, this reduction in the number of chloroplasts was also observed in *atapg9-1*, the loss of chlorophyll from each chloroplast was accelerated. In addition to that, morphology of the mesophyll cells was apparently different between wild-type and *atapg9-1* at 6 days after detachment. This result suggests that AtAPG9 is required for proceeding the leaf senescence process properly.

Even under nutrient growth conditions, the timing of bolting was accelerated in *atapg9-1* plants. I confirmed that the slight nitrogen starvation accelerated the timing of bolting in Arabidopsis. Considering together, even though enough nutrient is supplied, loss of AtAPG9 will cause the slight nitrogen starvation in plant .

These results indicate that autophagy is required for maintenance of the cellular viability during nutrient-limited conditions and leaf senescence. Efficient nutrient utilization within a whole plant can be achieved through such a vacuolar degradation process within cells.

Introduction

Protein degradation, vacuoles and autophagy

Protein degradation is an important process in many facets of plant physiology and development. In plants, two major degradation pathways have been described, the ubiquitin-dependent pathway and the vacuolar degradation pathway (for review see Vierstra, 1996). The ubiquitin/26S proteasome system contributes to the protein degradation in the cytoplasm and nucleus. The ubiquitin-dependent pathway requires that proteins targeted for degradation become conjugated with chains of multiple ubiquitins. These chains then serve as recognition signals for selective degradation by the 26S proteasome, a 1.5 MDa multisubunit protease complex. The ubiquitin pathway is particularly important for the selective degradation, such as degradation of cell-cycle regulators and transcription factors. On the other hand, vacuolar degradation is assumed to be involved in bulk protein degradation by virtue of the resident proteases in the vacuole. Two types of vacuole have been described in plants, the storage vacuole and the lytic central vacuole (for review see Marty, 1999). However, there may be additional vacuole types that await discovery. Protein storage vacuoles are often found in seed tissues and accumulate proteins that are mobilized and utilized as the main nutrient resource for germination. Most cells in vegetative tissues have a large central vacuole, containing a wide range of proteases in an acidic environment. Substrate proteins must be transported and sequestered into this vacuole for degradation. Autophagy, a ubiquitous eukaryotic process, is considered to play a major role for this sequestration.

Two types of autophagy exist in eukaryotes

Two types of autophagy have been described, namely macroautophagy and microautophagy (Figure 1 and for review see Klionsky and Ohsumi, 1999). In yeast macroautophagy, at first, a portion of the cytoplasm is enclosed by a double-membrane structure, the autophagosome (0.3-0.9 μm diameter). The outer membrane of the autophagosome then fuses to the vacuolar membrane, so that its inner membrane structure, the autophagic body, is delivered into the vacuolar lumen. The inner membrane and the contents of the autophagic body are then digested by vacuolar proteinases. In animal cells, the lysosome functions as the degradation compartment instead of the vacuole. The autophagosome (0.8-1.5

μm in diameter) fuses with a lysosome to become an autolysosome and its contents are digested by lisosomal proteinases. In microautophagy, the vacuolar membrane invaginates, directly enwraps the substrates, and is then pinched off. The enclosed cytoplasmic contents are then degraded inside the vacuole.

The autophagy genes are revealed in yeast

Macroautophagy in yeast have been studied intensely using *Saccharomyces cerevisiae*. The formation of autophagosomes is induced by nutrient starvation and addition of inhibitors or mutations in vacuolar proteinases cause the accumulation of autophagic bodies inside the vacuole. Using this accumulation of autophagic bodies as an indicator, a group of autophagy-defective mutants (*apg* and *aut*) were isolated (Tsukada and Ohsumi, 1993; Thumm et al., 1994). Most Apg/Aut proteins are directly involved in autophagosome formation. However, these mutants possessed functionally normal vacuoles. As a consequence of a specific defect in autophagy, all of these mutants display the following phenotypes: a defect in (i) bulk protein degradation induced by starvation, (ii) survival during starvation and (iii) sporulation of diploid cell. Through characterization of the Apg gene products, several molecular mechanisms essential for yeast autophagosome formation were discovered, such as the Tor-Apg1 phosphorylation system, PI3-kinase complex system, the Apg12 conjugation system and the Apg8 lipidation system (for reviews see Klionsky and Ohsumi, 1999; Ohsumi, 2001).

Orthologs of most Apg proteins were found in mammalian cells. Several sets of results indicate that the mammalian Apg proteins are also essential for autophagy in mammalian cells and that the molecular mechanism of autophagy is conserved among the different organisms (Kabeya et al., 2000; Liang et al., 1999; Mizushima et al., 1998b; Mizushima et al., 2001; Tanida et al., 1999).

Microautophagy have been studied mainly using the methylotrophic yeast, *Pichia pastoris*. Upon transfer from glucose to methanol medium, peroxisomal proteins and the peroxisomes themselves are induced in order to metabolize methanol. Upon shift back from methanol medium to glucose medium, the excess peroxisomes are degraded selectively by microautophagy. Sakai et al. isolated mutants defective in peroxisome microautophagy (*pag* mutants) (Sakai et al., 1998). Although some mutants affected in microautophagy are normal for macroautophagy, others are compromised in both autophagic processes. Thus, two different autophagic pathways share the common molecular machinery to some extent.

Autophagy is induced by starvation in plant cells

Processes analogous to macroautophagy and microautophagy in plant cells have been described in a number of morphological and biochemical studies (for reviews see Matile, 1975; Moriyasu and Hillmer, 2000). In suspension-cultured cells, autophagy is induced by sucrose starvation. In rice suspension-cultured cells, depletion of sugar induces the rapid consumption of cellular sugar and starch. Ultrastructural analysis indicates the degradation of cytoplasmic constituents including amyloplasts occurs inside the vacuoles (Chen et al., 1994). The mechanisms how amyloplasts are sequestered into vacuoles have not been revealed yet, however, they suggest that either macroautophagy or microautophagy must be involved.

In sycamore cultured-cells, incubation of cells in sucrose-free medium triggers a marked degradation of the membrane polar lipids. Interestingly, galactolipids, the lipids specific to the plastid envelope, are also severely affected by sugar starvation. In contrast, the total amounts of sterols, which are mainly associated with plasmalemma and tonoplast membranes, remains constant. During sucrose starvation, a massive regression of cytoplasm and typical macroautophagy is observed using electron microscopy. Double membrane-bounded vesicles (3-5 μm in diameter) are formed in the peripheral cytoplasm and eventually expelled into the central vacuole, which increases in volume and squeezes the thin layer of cytoplasm spared by autophagy (Aubert et al., 1996).

In tobacco suspension cultured-cells, net protein degradation is induced by sucrose starvation and protease activity in the cell increases 3- to 7- fold. When the cysteine protease inhibitor, (2S, 3S)-trans-epoxysuccinyl-leucylamido-3-methyl-butane (E64c), is added to the starvation medium, both the protein degradation and the increase in the protease activity are effectively inhibited. Light microscopic analysis showed that the accumulation of many small spherical bodies (1-6 μm in diameter) in the perinuclear region of the cytosol is induced by the inhibitor treatment. These spherical bodies are acidic inside and contained acid phosphatase activity, a maker enzyme of autolysosomes in mammalian cells (Dunn, 1990a, 1990b). As mentioned above, in yeast, protease inhibitor inhibits the disintegration of the autophagic bodies, and as a result, autophagic bodies accumulate in the central vacuole. So if vacuoles in plant cells work in the same way as yeast vacuoles during autophagy, some portions of cytoplasmic components are expected to accumulate in the vacuoles in the presence of protease

inhibitors. However, their results suggest that there may be lytic compartments other than the central vacuole that function in autophagy in tobacco cells (Moriyasu and Ohsumi, 1996).

When whole maize plants are submitted to prolonged darkness, soluble sugars drop sharply and significant decreases in protein level are observed. The increase in proteolytic activities is related to an enrichment of vacuolar protease, with no change in the amount of 20S proteasome, subcomplex of 26S proteasome. Ammonium and asparagine levels rise along with the protein degradation. This phenomenon is also observed in sucrose-starved sycamore suspension-cultured cells and this roughly accounts for the total nitrogen of proteins that disappear (Genix et al., 1990). These results suggest that dark-induced protein degradation is due to autophagic processes (Brouquisse et al., 1998).

Autophagy is observed during plant development

Autophagic processes are observed during several aspects of plant development. Many meristematic cells of higher plants appear to lack vacuoles. Although vacuoles are the most noticeable membrane-bounded organelles in differentiated plant cells, the question of their origin is unsettled. Marty reported involvement of autophagy in genesis of vacuoles. He investigated the pattern of vacuolation in root meristematic cells of *Euphorbia characias* L. by high-voltage and conventional electron microscopy (Marty 1978). The most undifferentiated root cells just adjacent to the quiescent zone are devoid of vacuoles or their identifiable precursors. In the cells where vacuolation is initiated, small vesicles, Marty mentioned as the primordial vacuole precursors or provacuoles, bud from the trans-Golgi network. The provacuoles are not seen budding from Golgi elements or from ER cisternae. In slightly more differentiated cells, provacuoles are elongated into tubes of 0.1 μm in diameter. Subsequently, several provacuolar tubes cooperate to drive a programmed cellular autophagy and merge to entrap the portion of cytoplasm in a double-membrane system. In more differentiated cells, the typical young vacuole is formed when the enclosed cytoplasm constituents and the inner membrane of the autophagic cavity are degraded. The young vacuoles fuse together and enlarge to give rise to a few large vacuoles. These vacuoles are able to engulf bits of cytoplasm by microautophagy and collect newly formed provacuoles by fusion of the respective membranes. He mentioned that the fate of provacuoles in

mature cells that are already vacuolated appears to be different from that in the immature, unvacuolated cells. Instead of participating in a programmed autophagic process, provacuoles in mature vacuolated cells directly fuse with the pre-existing large vacuoles.

Recently, an Arabidopsis mutant *vacuoless1* that lacks vacuoles was isolated (Rojo et al., 2001). Electron microscopic analysis revealed that in wild-type embryo cells, many small vacuoles are present in globular stage and as development proceeds, these small vacuoles fuse to form larger vacuoles. Whereas vacuoles are not present in *vacuoless1* mutant embryo cells, mutant cells accumulate many small vesicles in early-heart stage suspensor cells. The autophagosome compartments (1.2-1.8 μm in diameter) are observed in *vacuoless1* mutant embryo cells. During and after the heart stage, autophagosomes accumulate rapidly and by the late torpedo stage, cytoplasm is completely filled with autophagosomes. The macroautophagy may be induced by the lack of vacuole or autophagy may also occur in wild type embryo cells, while the short life span of autophagosomes may cause it difficult to detect autophagosomes in wild type embryo cells.

Autophagy is observed in legume cotyledon cells

Autophagy is also observed in legume cotyledon cells. Protein storage vacuoles contain the protein reserves of many seeds. During seedling growth the reserve proteins are catabolized within the protein storage vacuoles and protein storage vacuoles convert to lytic vacuoles. Ultrastructural observations of *Vigna radiata* cotyledon cells showed that protein storage vacuoles contain small vesicles (0.2-1.0 μm in diameter) with a cytoplasmic content such as ribosomes and mitochondria (van der Wilden et al., 1980). It is reasonable to suggest that these vesicles are formed by either microautophagy or macroautophagy. Toyooka et al. reported cotyledon cells of *Vigna mungo* use at least two distinct autophagic machineries (Toyooka et al., 2001). Ultrastructural analysis of cotyledon cells revealed that starch granules of the cotyledon cells are wrapped with the acidic compartments that would be formed by fusion of a de novo synthesized acidic vesicle and subsequently incorporated into the lytic vacuole. How wrapped starch granules are inserted into the inside of vacuoles is still not clear. However, they suggested that degradation of starch granules may be proceeded by a mechanism analogous to microautophagy. In addition to that, autophagosome-

mediated (0.2-0.5 μm in diameter) macroautophagy for cytoplasm and mitochondria is also detected in the cotyledon cells. When the embryo axes are removed from seeds and the detached cotyledons are incubated, the macroautophagy is observed, but the microautophagic process for the degradation of starch granules is not detected, suggesting that these two autophagic processes are regulated by different cellular mechanisms.

Autophagy is involved in leaf senescence

Senescence in plant is a well-organized developmental process and involves programmed cell death. It is known that the tonoplast rupture towards the last stage of programmed cell death and as a result, hydrolases are released from the vacuole, which digest the cell contents. Various kinds of hydrolytic enzyme accumulate in the vacuole during senescence in order to achieve a rapid degradation of the remaining cell constituents when vacuoles collapse (Matile 1997). However, several morphological studies have shown that vacuolar autophagy takes place during senescence (Matile and Winkenbach, 1971; Inada et al., 1998; Minamikawa et al., 2001).

Chloroplasts are protein-rich organelles in plants, containing most of the total cellular proteins in photosynthetic tissues. The degradation of chloroplast proteins during senescence has been interpreted from two points of view. One is that chloroplast proteins are degraded by proteolytic enzymes inside the chloroplast with the digestion products being exported. Proteolytic activities that reside in the stroma of chloroplasts are observed in a number of studies (Waters et al., 1982; Liu and Jagendorf, 1984; Mae et al., 1989; Musgrove et al., 1989; Bushnell et al., 1993; Shanklin et al., 1995). However, Miyadai et al. also reported that proteolytic activity against ribulose 1,5-bisphosphate carboxylase/oxygenase (Rubisco), one of the main chloroplast protein, found in lysates of mechanically isolated chloroplasts is mostly due to the contamination of vacuolar proteases adhering to the outer envelope of the chloroplasts during their isolation and involvement of active oxygen in the chloroplastic degradation of the Rubisco (Ishida et al., 1997; Miyadai et al., 1990).

The other viewpoint is that vacuole is the major intracellular compartment responsible for the chloroplast protein degradation. In mesophyll protoplasts of wheat and corn leaves, Rubisco-degrading proteases are localized in the vacuoles (Lin and Wittenbach, 1981). Thayer and Huffaker demonstrated vacuolar localization of

Rubisco-degrading endopeptidases in senescing barley leaf (Thayer and Huffaker, 1984). Degradation of Rubisco by vacuolar lysates prepared from wheat primary leaves and senescing French bean primary leaves is also reported (Bhalla and Dalling, 1986; Yoshida and Minamikawa, 1996)

To evaluate these two views on chloroplast protein degradation, a number of morphological studies dealt with the number and localization of chloroplasts during leaf senescence. However, the results are not necessarily consistent. Wardley et al. reported that chloroplast number per mesophyll cell of primary leaves of wheat remained essentially constant during senescence. It was not until more than 80% of the plastid chlorophyll and protein was degraded that some reduction (22%) in chloroplast number was recorded (Wardley et al., 1984). Thus, they conclude that degradation occurs within the chloroplast and that all chloroplasts in a mesophyll cell senesce with a high degree of synchrony rather than each chloroplast senescing sequentially. On the other hand, according to Wittenbach et al. there was a close correlation between the decline in chloroplast number and the loss of chlorophyll and soluble protein per mesophyll protoplast from senesing primary wheat leaves, suggesting a sequential degradation of chloroplasts during senescence (Wittenbach et al., 1982). Ultrastructural studies indicated a movement of chloroplasts toward the center of the protoplasts during senescence and thus, vacuolar uptake of chloroplasts was suggested. Ono et al. lead to the conclusion that chloroplast proteins are mobilized in two different ways during wheat primary leaf senescence, namely, by gradual degradation of the proteins inside the chloroplast and by the successive disappearance of a small population of whole chloroplasts (Ono et al., 1995). Recently, Minamikawa et al. showed that about 10% of chloroplasts in a cell of senescing French bean leaves are separated from the cytoplasm of the cell periphery and taken into the central vacuole (Minamikawa et al., 2001). Taken together, autophagic degradation of chloroplasts will be involved in senescence occurring under some, may be not all, conditions.

The aim of this study

Though autophagy-like phenomena were observed in a lot of aspects of plant life as described, how autophagy contributes to plant life is still to be determined. In addition, little is known about the molecular mechanisms involved in autophagy in plant cells. This must be due to a current lack of knowledge regarding genes involved in autophagy

and autophagy-related mutant plants. From this point of view, I decided to start the study of autophagy in plant cells by the aid of molecular biological approaches for the first time, and three points were set as the aim of my research. The first aim is to identify genes involved in plant autophagy. The second aim is to isolate autophagy gene mutant plants and elucidate the physiological roles of autophagy in plant by analysis of their phenotypes. The third aim is to elucidate the molecular functions of plant autophagy genes in plant cell autophagy.

MATERIALS AND METHODS

Plant material and culture conditions

All experiments were performed using *Arabidopsis thaliana* ecotype Wassilewskija (WS), except for isolation of the *AtAPG* cDNA clone, which was from *Arabidopsis thaliana* ecotype Columbia. The plants were grown on rockwool using vermiculite as soil at 22 °C with 16 h light/8 h dark cycles, using hydroponic media as nutrient solution. Alternatively, the hydroponic culture was carried out as described in Hirai et al. (Hirai et al., 1995). Briefly, hydroponic cultures were initiated by putting 10-day old seedlings on floats in hydroponic media. The media were aerated and changed twice per week. The hydroponic media contained 1.5 mM NaH_2PO_4, 0.26 mM Na_2HPO_4, 1.5 mM $MgSO_4$, 2.0 mM $Ca(NO_3)_2$, 3.0 mM KNO_3, 30 μM H_3BO_3, 8.7 μM NaFe-EDTA, 10.3 μM $MnCl_2$, 1.0 μM $ZnCl_2$, 1.0 μM $CuCl_2$, 130 nM $CoCl_2$, and 24 nM $(NH_4)_6Mo_7O_{24}$.

For carbon starvation, 7-day old seedlings grown on rockwool were subjected to 24 h dark conditions.

For root elongation analysis, plants were grown on vertical positioned 1/2 concentration MS plates with or without 2 % sucrose.

For nitrogen starvation in hydroponic culture, 10-day old seedlings grown on rockwool were transferred to nitrogen-depleted medium and grown hydroponically. A nitrogen-depleted medium was prepared by replacing KNO_3 and $Ca(NO_3)_2$ with KCl and $CaCl_2$, respectively.

For analysis of effects of nitrogen starvation on the bolting time, plants were grown using rockwool and vermiculite and nitrogen was supplied as nutrient solution. Three solutions of different nitrogen concentration were prepared by the same way as nitrogen starvation medium for hydroponic culture.

Arabidopsis suspension-cultured cells

Arabidopsis suspension-cultured cells used in this study were maintained by passaging 6 ml of the cell suspension in stationary phase to 50 ml of fresh MS medium containing 3 % (w/v) sucrose every week. Cultures were grown in flasks at 22 °C with a rotation.

Cloning of *AtAPG* genes

Genes homologous to *S. cerevisiae APG* were searched for in the Arabidopsis ecotype Columbia EST and genomic databases using the BLAST program. *AtAPG* cDNA sequences were determined by various methods. RT-PCR was performed to amplify the predicted coding region for *AtAPG3, 4a, 4b, 5, 7, 8a, 8b, 8c, 8d, 8e, 8f, 8g, 8h, 8i, 9, 12a* and *12b*. Primer sequences used for the cloning of *AtAPG* genes were as follows.

AtAPG3 specific primers: 5'-ATGGTGCTTTCGCAAAAGCTTCATGAAGCA-3' and 5'-TTATGTACAGTGCAGAGCCATCCAGCC-3'.

AtAPG4a specific primers: 5'-ATGAAGGCTTTATGTGATAGATTTGTTC-3' and 5'-TCAGAGCATTTGCCAGTCATCTTCAC-3'.

AtAPG4b specific primers: 5'-CGgaattcGTTGTATTTGGTGCTTAATGA-3' and 5'-gtcacacaatgaaaagaatggctaggag-3'.

AtAPG5 specific primers: 5'-TCCcccgggATGGCGAAGGAAGCGG-3' and 5'-GCtctagaTCACCTTTGAGGAGCTTTC-3'.

AtAPG7 specific primers: 5'-ATGGCTGAGAAAGAAACTCCAGCAATC-3' and 5'-TTAAAGATCTACAGCTACATCGTCATCATC-3'.

AtAPG8a specific primers: 5'-tcggagactaatcgaatcgc-3' and 5'-catcaaagtcatccaaagatcg-3'.

AtAPG8b specific primers: 5'-catcgtagatactaaccgaatcatc-3' and 5'-GATCAGACGTAGAAGCTGAGG-3'.

AtAPG8c specific primers: 5'-aatcttTGATtctttaatcgcc-3' and 5'-caaagcaacatTTAcattaatagtag-3'.

AtAPG8d specific primers: 5'-tctcttctctgtttctctctcg-3' and 5'-tcgatccacatattccaagc-3'.

AtAPG8e specific primers: 5'-ttccatcaaattctctctctaag-3' and 5'-cggattctcagaggtcagag-3'.

AtAPG8f specific primers: 5'-gtagtctacaggcgtggaagg-3' and 5'-TTATGGAGATCCAAATCCAAATG-3'.

AtAPG8g specific primers: 5'-cgcataatccagagaggacc-3' and 5'-cattcaattaaaagcaagaacacc-3'.

AtAPG8h specific primers: 5'-tcattcgtcgtgaaatctg-3' and 5'-aaatcttttgTTAgccgaaag-3'.

AtAPG8i specific primers: 5'-ccgggcggtcgaagaag-3' and 5'-acacagacactaacatcattattgg-3'.

AtAPG9 specific primers: 5'- ATGAGCAGTGGGCATAAGGGTCCAAATG-3' and 5'-TCACCGTAATGTGGTGCTTGATGTTG-3'.

AtAPG12a specific primers: 5'-cgGAAttcttcattcagttaCGAAAACC-3' and 5'-TTAGCCCCATGCCATGGAACAAGC-3'.

AtAPG12b specific primers: 5'-aacaatggcgaccgaatctccgaat-3' and 5'-tcagagattgatgacgaagttttaac-3'.

Each cDNA was obtained from PCR products using the Marathon cDNA amplification kit (CLONTECH, Palo Alto, CA) and subcloned into pBluescript SK+ (STRATAGENE, La Jolla, CA). Each cDNA was then sequenced, and the sequences were deposited into DDBJ/NCBI/EMBL. For *AtAPG1a, AtAPG5* and *AtAPG6*, a cDNA sequence had previously been deposited by other groups. For *AtAPG1b, 1c, 2, 10, 13a* and *13b*, coding regions were predicted based upon a comparison of the Arabidopsis genomic DNA sequence with several APG homologs from other organisms. A splicing site prediction program was also used.

Accession number for the *AtAPG* sequences are: *AtAPG1a* (AAK59554), *AtAPG3* (AB073170), *AtAPG4a* (AB073171), *AtAPG4b* (AB073172), *AtAPG5* (AI997825), *AtAPG6* (AAK62668), *AtAPG7* (AB073173), *AtAPG8a* (AB073175), *AtAPG8b* (AB073176), *AtAPG8c* (AB073177), *AtAPG8d* (AB073178), *AtAPG8e* (AB073179), *AtAPG8f* (AB073180), *AtAPG8g* (AB073181), *AtAPG8h* (AB073182), *AtAPG8i* (AB073183), *AtAPG9* (AB073174), *AtAPG12a* (AB073184) and *AtAPG12b* (AB073185). The rest of the AtAPG protein sequences are predicted based upon genome sequence. Accession numbers for the corresponding BAC clones are: *AtAPG1b* (AL132960), *AtAPG1c* (AC007661), *AtAPG2* (AP000419), *AtAPG10* (AC009853), *AtAPG13a* (AL132964) and *AtAPG13b* (AB026654).

Software programs

Amino acid sequence alignment was performed using the program Megalign (DNASTAR, Madison, WI). Hydrophilicity analysis was performed using Protean (DNASTAR).

Complementation test of yeast *apg* mutants with *AtAPG* genes

To express AtAPG proteins in yeast, each *AtAPG* genes were inserted under the GAP promoter of the yeast expression vector pKT10 (Tanaka et al., 1990). Yeast strains were grown in standard rich medium (YPD) or starvation medium as described previously (Noda et al., 2000). Yeast strains used in the complementation test were

described in following references: *Δapg3* (Ichimura et al., 2000), *Δapg4* and *Δapg8* (Kirisako et al., 2000), *Δapg5, Δapg7* and *Δapg12* (Mizushima et al., 1998a), *Δapg9* (Noda et al., 2000) and *Δapg10* (Shintani et al., 1999).

Yeast whole-cell lysates were prepared by breaking the cells with 0.2 N NaOH, 1 % 2-mercaptoethanol. Then proteins were precipitated by addition of TCA and after centrifugation, samples were washed with cold aceton and subjected to the 9 % polyacrylamide SDS-PAGE and analysed by immunoblotting using ant-API antibody. Anti-API antibody was previously described (Noda et al., 2000).

Western blotting of AtAPG9

Anti-AtAPG9 antibody against His-tagged AtAPG9 was prepared by immunization of rabbits and affinity purified. To produce His-tagged AtAPG9, the part of *AtAPG9* cDNA fragment encoding C-teminus 247 amino acids was prepared by *Hind*III digestion. This fragment was cloned into expression vector, pET28b (Novagen) digested with *Hind*III. The resulting plasmid pHH20 was expressed in E. coli and obtained His-tagged AtAPG9 recombinant proteins were purified by Ni column.

Plant protein samples were prepared as follows: plant aerial parts were homogenized in extraction buffer (50 mM HEPES-KOH, pH 7.5, 10 mM KOAc, 1 mM EDTA, 0.4 M sucrose, 1 mM DTT, 2 mM PMSF and 5 % plant protease inhibitor cocktail (SIGMA P-9599)). The lysate was centrifuged at 4 °C, 1000 x g, for 10 min. The pellet was discarded, and the supernatant was then ultracentrifuged at 4°C, 100,000 x g, for 1 h. The pellet (ppt) and the supernatant (sup) were analysed by SDS-PAGE, followed by immunoblotting.

Yeast whole-cell lysates were prepared in the same way as complementation test of yeast *apg* mutants with *AtAPG* genes.

Screening of T-DNA insertion lines

I used the T-DNA insertion-line screening system engineered at the Kazusa DNA Research Institute (Kazusa, Japan). The principles of the screening method have been previously described (McKinney et al., 1995). *AtAPG9* specific primers used for screening were 5'- ATGAGCAGTGGGCATAAGGGTCCAAATG-3' and 5'-TCACCGTAATGTGGTGCTTGATGTTG-3'. The T-DNA specific primers were 5'-TAGATCCGAAACTATCAGTG –3' and 5'- ATAACGCTGCGGACATCTAC –3'. We

used four combinations of primer sets, each consisting of a gene-specific primer and a T-DNA specific primer. The position of the T-DNA insert was determined by sequencing the PCR products carrying the T-DNA-genome junctions.

Southern blot analysis

Total genomic DNA isolated from wild-type and mutant Arabidopsis was digested with various restriction enzymes and subjected to southern-blot analysis following standard protocols for the DIG system (Roche Diagnostics, Tokyo, Japan). Digoxigenin-labeled cauliflower virus 35S promoter probes or *AtAPG9* probes were prepared by PCR. The specific primers for 35S promoter were 5'-TGGAGCACGACACGCTTG-3' and 5'-AGATATCACATCAATCCAC-3'. The *AtAPG9* specific primers were 5'-GATATTCGGATGCATGTAC-3' and 5'-CCCATTGGATCCCTGG-3'. Digoxigenin-labeled probes were hybridized to the membrane-bound DNA at 42 °C in 5x SSC (20x SSC = 3 M NaCl and 0.3 M sodium citrate), 0.1% N-lauroylsarcosine, 0.02% SDS, 1% blocking reagent and 50% (v/v) formamide. Washing was performed at 68 °C in 0.1x SSC and 0.1% SDS and the blots were analyzed for chemiluminescence.

RT-PCR to verify *AtAPG9* expression

Total RNA was extracted from each samples using ISOGEN (NIPPON GENE, Tokyo, Japan), and first-strand cDNA was generated using the ProSTAR RT-PCR kit (STRATAGENE) following the manufacturer's instructions. For PCR, *AtAPG9* specific primers (5'-TTGGATCTTTTTGTCGAAAGGCTCTAC-3' and 5'-AAAG-CTGCAAACATGGCCTACACC-3') and Arabidopsis *ACTIN2* specific primers (5'-ATGAAGATTAAGGTCGTTGCACCACC-3' and 5'-CTTATATTAACATTG-CAAAGAGTTTCAAGG-3') were used.

Complementation test of *atapg9-1*

The *AtAPG9* gene, including 3 kbp upstream from the start codon, was amplified by PCR from genomic DNA using two sets of primers, 5'- ACCGCTCGAGTTTT-CAACTGGTTTCCTTC-3' and 5'-GCGGATCCCAGAGAAGCATATGATG-3' or 5'-TTGGATCTTTTTGTCGAAAGGCTCTAC-3' and 5'-AGTCGAGCTCACCG-TAATGTGGTGCTTGA-3'. The 1st amplified fragment, attained using the former set of primers, was cloned into pBluescript KS+ digested with *Eco*RV. The resulting

plasmid pHH34 was digested with *Nde*I and *Sac*I and subsequently ligated with the 2nd amplified fragment digested with *NdeI*/*Sac*I. Next, the *Xho*I-*Sac*I fragment was cloned into the binary vector pBI121Δ35S, a derivative of pBI121 (Hayashi et al., 2000). The resulting plasmid pHH38 was introduced into the *Agrobacterium* strain C58C1Rif', which was then used to transform the Arabidopsis *atapg9-1* homozygous mutant by the floral dip method (Clough and Bent, 1998). Transgenic plants were identified by kanamycin resistance. Seven T1 plants were selected and the T2 generation was screened for 3:1 (resistant : non-resistant) segregation. Two of these plant lines showed 100% resistance to kanamycin in the T3 generation, and these were selected as homozygous plant lines. The homozygous T3 and T4 plants were used for the following physiological experiments.

Transient expression in onion epidermal cells

Onion epidermal cells were used for particle bombardment. Onion epidermal cells were placed onto MS medium prior to bombardment. Each sample was then bombarded with gold particles (1 μm in diameter) coated with plasmids encoding green fluorescent protein (GFP) or AtAPG9-GFP. To prepare the plasmid encoding AtAPG9-GFP, *AtAPG9* cDNA was amplified by PCR using a set of primers 5'-gagcCTCGAGatgagcagtgggcataag-3' and 5'-gtacCCCGGGCccgtaatgtggtgcttg-3' and after digestion with *Xho*I and *Sma*I, amplified fragment was cloned into pEZS-NL (Cutler et al., 2000) digested with *Xho*I and *Sma*I. Biolistic PDS-1000/He Particle Delivery System (Bio-Rad) was employed at 1,100 psi at 9 cm distance. After bombardment, samples were incubated at 23 °C for 24 hr under continuous light and then subjected to the microscopic analysis using a fluorescence laser scanning confocal microscope, LSM510 (Carl Zeiss, Inc.).

Determination of chlorophyll content

Chlorophyll was extracted from fresh cotyledons or 1st and 2nd rosette leaves with methanol at 4°C for 1 day. The extracts were subjected to spectrophotometric measurements at 625, 647 and 664 nm. Chlorophyll contents were calculated using a Moran equation (Moran, 1982).

Measurement of cellular fresh weights

Cells in 3 ml of suspension were collected on a filter paper (55 mm in diameter) using vacuum filtration. The weight of filter paper with cells was measured, and the fresh weight of the cells was calculated by subtracting the weight of a filter paper.

Sucrose starvation of the suspension-cultured cells or Arabidopsis root cells

For the cultured cells, four day old, logarithmically growing cells were collected by centrifugation at 100 g for 4 min. Cell pellets were resuspended in MS medium without sucrose, and after an additional centrifugation step the cells were suspended in the original volume of MS medium without sucrose. The resultant cell suspension in the starvation medium was incubated in flasks at 22 °C with a rotation. Protease inhibitors were added from stock solutions (x 1000) in DMSO.

For the root cells, plants were grown on MS medium with 2 % sucrose for 7 days, and then roots were excised at about 3 mm long from the top and incubated in the liquid MS media (0 % sucrose) with or without E64d.

Vital staining with quinacrine or neutral red

Cells in 500 µl of suspension medium or root segments were washed by centrifugation through 5 mM Hepes-Na (pH 7.5) containing 0.1 M sorbitol. The samples were stained in the same solution containing 40 µM quinacrine or 35 µM neutral red for 5 min at room temperature. The samples were washed again with the same solution and observed using a fluorescence laser scanning confocal microscope.

Analysis of floral transition time

The plants were grown on rockwool using vermiculite as soil. Floral transition time was scored as the time at which the main inflorescence shoot had elongated to 5 mm.

Artificial induction of leaf senescence

The third and the fourth rosette leaves of 3-week old plants were detached and floated on deionized water in 12-well Petri dishes, abaxial side up (Oh et al., 1996). Leaves were incubated at 22 °C in the dark.

Microscopic analysis of leaf mesophyll cells

About 3 mm square leaf segments were prepared by the razor. Then leaf segments were placed in the 10 ml syringe and given pressure to absorb the water. After the absorption of the water, segments were observed using a fluorescence laser scanning confocal microscope.

RESULTS

Identification of Arabidopsis *AtAPG* genes

To identify homologs of yeast *APG* genes in Arabidopsis, I searched the Arabidopsis EST and genomic databases using BLAST. The search successfully identified 25 genes that encode proteins with significant homology to 12 of the 15 yeast Apg proteins. Homologs of the remaining 3 Apg genes (Apg14, Apg16 and Apg17) have thus far not been found in other organisms, suggesting that these molecules are not well-conserved in amino acid sequences between different oraganisms. All 25 genes are novel ones that are not yet described. At the present time, 23 of the 25 corresponding EST or cDNA clones have been deposited in the NCBI/EMBL/DDBJ database (with the exception of *AtAPG2* and *AtAPG10*). However, ESTs corresponding to *AtAPG2* and *AtAPG10* were found in other plant species as well. Then I cloned most of the cDNAs by RT-PCR and 5'/3'-RACE, and determined their intron/exon boundaries by comparing genomic sequences with the corresponding cDNAs. In many cases, the predicted coding sequences annotated in the database were not correct.

Figure 2 shows a diagram comparing yeast Apg proteins and Arabidopsis AtAPG proteins. Not only do all of the AtAPG proteins show significant homology to yeast Apg proteins, but the functional domains and essential amino acid sequences of the yeast Apg proteins are also well-conserved as follows.

Three Arabidopsis proteins (AtAPG1a, AtAPG1b and AtAPG1c) were assigned to Apg1p, a protein kinase whose activity is essential for autophagy (Matsuura et al., 1997). All AtAPG1 proteins contain an N-terminal kinase domain with a high degree of similarity to Apg1p, in addition to a less homologous region in the C-terminal half. Apg13p, the regulatory subunit of Apg1 kinase (Funakoshi et al., 1997; Kamada et al., 2000), displayed overall homology with AtAPG13a and AtAPG13b.

In the yeast Apg12 conjugation system, the C-terminal glycine of Apg12p is conjugated to a lysine residue of Apg5p via an isopeptide bond in a ubiquitination-like manner. This conjugation reaction is mediated by Apg7p, a ubiquitin-activating enzyme (E1)-like protein, and by Apg10p, a ubiquitin-conjugating enzyme (E2)-like protein (Mizushima et al., 1998a; Tanida et al., 1999; Shintani et al., 1999). Lys 149 of Apg5p, essential for Apg5/Apg12 conjugation, corresponds to Lys 128 of AtAPG5. Both the ATP-binding motif Gly-X-Gly-X-X-Gly and Cys 507 of Apg7p, which are

essential for E1-like activity, are conserved in AtAPG7. Cys 133 of Apg10p, at the active site of Apg10p, corresponds to Cys 178 of AtAPG10. The C-terminal Gly of Apg12p, through which Apg12p is covalently attached to Apg5p, is conserved in both AtAPG12a and AtAPG12b.

In the Apg8 lipidation system, another ubiquitin-like system essential for autophagy, the Apg4p protease removes the carboxyl-terminal Arg of Apg8p and leaves a Gly residue at the C-terminus of Apg8p. Apg8p is then activated by Apg7p and is subsequently attached to Apg3p, another E2-like enzyme after which the C-terminal Gly of Apg8p is conjugated to phosphatidylethanolamine by an amide bond and Apg8p is bound to membranes. Finally, Apg8p is reversed to soluble or loosely membrane-bound form by removal of phosphatidylethanolamine by Apg4p (Kirisako et al., 2000; Ichimura et al., 2000). Comparison of these four Apg8 system proteins (Apg3p, -4p, -7p, and -8p) with their Arabidopsis counterparts again revealed a considerable number of conserved essential residues. Cys 234 of Apg3p corresponds to Cys 258 of AtAPG3, which serves as an active site to catalyze the E2-like reaction in the Apg8 lipidation system. Cys 159 of Apg4p, which functions as the catalytically active amino acid for processing of Apg8p, aligns with Cys 170 of AtAPG4a and Cys 173 of AtAPG4b.

Nine homologs of Apg8 were found in the Arabidopsis genome. All of them display an extremely high degree of identity (~70%) with yeast Apg8p and contain Gly at their carboxyl end (Fig. 3). Two of nine homologs, AtAPG8h and AtAPG8i, do not possess an extra amino acid tail downstream of the conserved Gly. The biological meaning of this gene duplication is still unclear. It may indicate the existence of a number of subtly different autophagy pathways in plants that may have their own organ-specific function. In fact, immunoblotting of AtAPG8 using antibody against yeast Apg8p revealed an organ-specific banding pattern (data not shown). Further characterization of each AtAPG8 molecule will hopefully yield answers to this interesting question.

Recently, the candidate of functional homolog of Apg16, named as p63, was identified in mammalian cells (Kobayashi et al., personal communication). There is one homolog of p63 in Arabidopsis genome. This gene product may also serve as functional homolog of Apg16 in plant cell autophagy.

Clearly, this genome-wide scan has revealed a remarkable level of conservation in

APG gene family between yeast and higher plants.

Complementation test of yeast *apg* mutants with *AtAPG* genes

In yeast, aminopepetidase I (API) is synthesized in the cytosol as a precursor enzyme, prAPI (61 kDa). Under starvation conditions, prAPI is transported to the vacuole via autophagy where it is processed, in a proteinase A dependent manner, to mature API (mAPI, 50 kDa) (Fig. 4A). So the autophagic activity can be assessed by API maturation. Thus, I checked if AtAPG proteins could complement the defect of API maturation in corresponding yeast *apg* mutants. This complementation test was performed with AtAPG3, 4a, 4b, 7, 9,12a and 12b. Each *AtAPG* gene was cloned into pKT10 vector which enables them constitutive expression in yeast cells (Tanaka et al., 1990). Yeast cells deleted of apg3, apg4, apg7, apg9 and apg12 were transformed with the pKT10 based respective AtAPG genes. The cells were grown in synthetic medium + 2% dextrose and casamino acid to the log-phase, and harvested. Then they were disrupted by alkali method and lysates were subjected to western blotting with anti-API antibody. As shown in Figure 4B, immunoblotting of API revealed that mature API were formed in yeast *apg4* mutants expressing *AtAPG4a* or *AtAPG4b*, indicating that both AtAPG4a and AtAPG4b could complement the autophagic defect of the yeast *apg4* mutation. Microscopic analysis also showed the autophagic activity was restored partially in *apg4* mutants expressing *AtAPG4a* or *AtAPG4b* (data not shown). As none of the mammalian Apg homologs tested so far were capable of complementing the yeast *apg* mutations, AtAPG4a and 4b are the first Apg homologs from a multi-cellular organism which could complement the biological function of yeast Apg proteins. Other AtAPG proteins tested here could not complement the autophagic defect of the corresponding yeast *apg* mutants.

Identification of *atapg9-1*, a T-DNA insertional *AtAPG9* mutant

To investigate the physiological role of autophagy in higher plants, I screened the Arabidopsis Biological Resource Center and Kazusa DNA Research Institute T-DNA insertion lines for *AtAPG* knockout mutants. For analysis of autophagy-defective plant mutants, knockout plants of *AtAPG* genes that exist as a single copy in the Arabidopsis genome were desired. With this criterion, an Arabidopsis line carrying the T-DNA insertion within the third intron of *AtAPG9* was identified (Fig. 5A). Sequencing of

the genomic PCR products carrying the T-DNA-genome junction revealed that the 3'-half of *AtAPG9* was lost and replaced by the T-DNA. The segregation pattern of antibiotic resistance indicated that this line carries a single T-DNA insertion, an assumption which was confirmed by southern blot analysis using internal sequence of the T-DNA insertion as a probe (Fig. 5B). The disruption of the *AtAPG9* gene by T-DNA insertion in *atapg9-1* was further confirmed by southern blot analysis using *AtAPG9* as a probe (Fig. 5C). The band pattern of *atapg9-1* completely differed from that of wild-type. I designated this line *atapg9-1*. A single hybridized band pattern for each of the restriction enzymes tested indicates that *AtAPG9* is a single copy gene in the Arabidopsis ecotype WS genome (Fig. 5C). Upon completion of the genome sequence project, the lack of other Apg9 homolog in the Arabidopsis ecotype Columbia genome was also confirmed.

Expression of *AtAPG9*, *AtAPG9* mRNA was not detected in *atapg9-1* mutant

To confirm the effect of T-DNA insertion on *AtAPG9* expression in *atapg9-1* mutant, RT-PCR was performed using *AtAPG9* specific primers. At first, the organ specificity of *AtAPG9* expression was investigated. The total RNA was prepared from each organ of plant grown in hydroponic culture for 1 month. Though the expression level in root was lower than other organs, the *AtAPG9* transcript was detected in all tested organs: namely leaf, stem, flower and root (Fig. 6A).

Then, I checked the *AtAPG9* expression in *atapg9-1* plants using total RNA prepared from whole aerial parts as a template. As a result, no *AtAPG9* transcript was detected in the homozygous *atapg9-1* plants (Fig. 6B). This data confirms that *atapg9-1* contains a null mutation of the *AtAPG9* gene. After three successive backcrosses to the wild-type, the homozygous *atapg9-1* plants were propagated for further study.

As assurance that our experimental results were the direct effect of null mutation of the *AtAPG9* gene, I transformed *atapg9-1* plants with wild-type *AtAPG9*, including its own promoter. In mutant plants containing the wild-type *AtAPG9* transgene, the expression of *AtAPG9* was restored (Fig. 6B).

Characterization of APG9 homologs

Figure 7A shows the amino acid alignment of the Apg9 homologs found in Arabidopsis and other organisms. I noticed that there is a highly conserved region corresponding to AtAPG9 Trp 206-Gly 549. Yeast Apg9p was suggested to be an integral membrane protein (Noda et al., 2000), and hydrophilicity analysis of the APG9 homologs showed the conserved region corresponds well to the multi-membrane-spanning domains of the middle region (Fig. 7B). On the other hand, the NH_2- and COOH- terminal hydrophilic domains were somewhat divergent between the species.

Then I raised anti-AtAPG9 antibody. The *AtAPG9* cDNA contains an open reading frame encoding for a hydrophobic protein of 866 amino acids. The antibody was raised against recombinant protein corresponding soluble region of AtAPG9 (C-terminus 247 amino acids). The part of *AtAPG9* cDNA fragment encoding C-teminus 247 amino acids was cloned into expression vector, pET28b (Novagen). The His-tagged AtAPG9 recombinant proteins were expressed in E. coli and purified by Ni column. Anti-AtAPG9 antibody was prepared by immunization of rabbits and affinity purified. By western blot analysis, the antibody recognized the specific band of predicted size (99 kDa) in lysate prepared from yeast *Δapg9* cells expressing AtAPG9 (Fig. 8A). However, in plant samples, the antibody recognized a band of only 47 kDa. This 47-kDa band was not detected in the protein sample prepared from *atapg9-1* plant (Fig. 8B). These results suggest that AtAPG9 protein is prone to degradation during sample preparation. In this experiment, the putative AtAPG9 degradation products were detected both in soluble fraction (sup) and membrane fraction (ppt). I thought even though AtAPG9 originally existed in the membrane fraction, the degradation of AtAPG9 caused the soluble region of AtAPG9 moved to the soluble fraction.

AtAPG9-GFP was localized to dot structures in the cytosol

To assess the cellular localization of AtAPG9, I examined localization of fusion protein of AtAPG9 with GFP in onion epidermal cells (Fig. 9). The plasmid encoding GFP or AtAPG9-GFP was introduced into onion epidermal cells by particle bombardment. Both *GFP* and *AtAPG9-GFP* expression were driven by cauliflower mosaic virus 35S promoter and microscopic observation was carried out 1 day after bombardment. While cells expressing GFP showed nucleus and cytosolic pattern (observed as vacuolar

strands)(Fig. 9B and D), the fluorescence pattern was observed as moving dots in the cell expressing AtAPG9-GFP (Fig. 9F and H). These dots were always observed on weakly fluorescent vacuolar strands, indicating that these dot structures were localized in the cytosol, not vacuole. In onion epidermal cells, a lot of small particles in motion were observed in differential interference microscope image, possibly plastids or mitocondria (Fig. 9G and I). However, the observed dot structures of AtAPG9-GFP didn't colocalize with these particles (Fig, 9K).

Accumulation of lytic spherical bodies was induced in Arabidopsis cultured cells by addition of the cysteine protease inhibitor

I checked if lytic spherical bodies accumulate in sugar-starved Arabidopsis suspension-cultured cells by addition of the cysteine protease inhibitor as in tobacco suspension-cultured cells (Moriyasu and Ohsumi, 1996). The cells were transferred to fresh medium every 6 or 7 days and four-day-old, logarithmically growing cells were subjected to the following analysis. First, the staining pattern of two acidtropic dyes, quinacrine (QUI) and neutral red (NR) were checked. As shown in Figure 10A-F, these dyes stained central vacuoles well. Next, morphological changes of Arabidopsis suspension-cultured cells during sugar starvation were investigated. Suspension-cultured Arabidopsis cells (maintained in MS medium with 3% sucrose) usually contain many amiloplast like structures (Fig. 10A and D). After the transfer to the starvation medium (MS medium without sucrose), gradually amiloplast like structures were lost and large central vacuole was developed (Fig. 10G). When E-64d, cysteine protease inhibitor, was added to the starvation medium, the accumulation of spherical bodies was observed after the loss of amiloplast like structures in 1 day (Fig. 10J). Quinacrine and neutral red, both dyes staine an acidic compartment, stained these spherical bodies strongly (Fig. 10K and L), suggesting these spherical bodies were the same structures observed in tobacco suspension-cultured cells. These spherical bodies mainly accumulated perinuclear region and most of them didn't show movement. However, small groups of spherical bodies which didn't exist near the nucleus as the large assemblage showed some movement (arrows in Fig. 10J).

Accumulation of lytic spherical bodies was induced in Arabidopsis root by addition of the cysteine protease inhibitor

As I ensured accumulation of spherical bodies in Arabidopsis cultured cells, next I checked if the same phenomenon was observed in Arabidopsis root cells (Fig. 11). Plants were grown on MS medium with 2 % sucrose for 7 days, and then roots were excised at about 3 mm long from the top and incubated in the liquid MS media (0 % sucrose) with or without E-64d. As a result, accumulation of spherical bodies was observed when root segments were incubated with E-64d for more than 5 hours (Fig. 11C). As shown in Figure 11F, these spherical bodies were stained strongly with neutral red.

In addition to that, small particles were often observed in the central vacuole even without E-64d treatment (arrows in Fig. 11A and B). These particles were also stained with neutral red (data not shown).

Accumulation of lytic spherical bodies was reduced in *atapg9-1*

Next, I checked if the accumulation of these spherical bodies was affected in *atapg9-1* mutant plants. As shown in Figure 12, although some spherical bodies were also observed in *atapg9-1* root cells, the number of spherical bodies were apparently reduced in *atapg9-1* compared to wild-type plants. These spherical bodies were suggested as the degradation compartments other than the central vacuole, namely autolysosome-like structures, functioning in plant cell autophagy (Moriyasu and Ohsumi, 1996). This result strongly supports the idea that AtAPG9 plays important role in the autophagy pathway in Arabidopsis cells.

Under nitrogen starvation, chlorosis was proceeded rapidly and seed production was affected in *atapg9-1* plants

Autophagy is known to be induced in nutrient starvation. So I subjected the *atapg9-1* mutant plants to nutrient deficient conditions and checked their phenotypes. First, growth under nitrogen starvation conditions was observed. For nitrogen starvation, 10-day old seedlings grown in nutrient medium (7 mM nitrate) were transferred to nitrogen-depleted medium (0 mM nitrate). Nitrate was the sole nitrogen source of the culture media used in this study. During 14 days of nitrogen starvation, chlorosis of the cotyledons and 1st and 2nd rosette leaves was proceeded more rapidly in *atapg9-1* than wild-type (Fig. 13A). The chlorophyll content was measured after removal of nitrogen. The amount of chlorophyll per fresh weight (FW) was similar in both wild-type and *atapg9-1* plants at day 0, implying that chlorophyll synthesis was not affected by the *atapg9-1* mutation. Time course analysis indicated that the rate of chlorophyll degradation from 3 day to 14 day in *atapg9-1* 1st and 2nd rosette leaves was 20% higher than in wild-type leaves (Fig. 13B).

Additionally, *atapg9-1* plants could not produce as many seeds as wild-type plants. As shown in Figure 14A, wild-type plants could bear mature silique even in 5th and 6th flowers, whereas most of *atapg9-1* plants could not. Most *atapg9-1* plants produced only 4 flowers, thus the average number of mature silique per mutant plant was less than that of wild-type (Fig. 14B). Both the chlorophyll content in rosette leaves after 14 days of nitrogen starvation and seed production were restored to the corresponding wild-type levels in mutant plants expressing transgenic wild-type *AtAPG9* (Fig. 13A, C and Fig. 14). Judging from these results, it is clear that AtAPG9 is of vital importance for efficient utilization of nitrogen when its supply is restricted.

Chlorosis of cotyledon was induced rapidly in *atapg9-1* plants under extended darkness

Growth under carbon starvation was also observed. For carbon starvation, 7-day old seedlings grown on rockwool with 16 h light/8 h dark cycles were transferred to 24 h dark conditions. The chlorophyll content was measured after removal of light (Fig. 15A). In dark-incubated plants, the chlorophyll content of cotyledons started to decrease, and at day 9, it became half of its starting level. However, in *atapg9-1*, only half level of wild-type chlorophyll content was left at day 9. Figure 15B shows a

photograph of the plant after 8 days of carbon starvation. The *atapg9-1* cotyledons turned yellow while those of the wild-type plants retained a pale green color. This phenotype was restored by complementation with wild-type *AtAPG9* expression (Fig. 15B and C), indicating that AtAPG9 is important for cell survival under carbon starvation conditions.

Root elongation was affected by sucrose supply in *atapg9-1*

The involvement of autophagy in formation of vacuoles in the root cells was reported (Marty 1978). So I checked root elongation in *atapg9-1*. Wild-type and *atapg9-1* plants were grown on the 1/2 MS medium with or without 2% sucrose at 22 °C with 16 h light/8 h dark cycles. The root length was measured 4 days after germination. As shown in Figure 16A, the root elongation was not affected in *atapg9-1* when sucrose existed in the medium. However, on sucrose depleted medium, root elongation was severely inhibited in *atapg9-1*. Figure 16B showed ratio of root length on the sucrose depleted medium to the root length on the sucrose containing medium. While, sucrose depletion did not affect so much the elongation of the root in wild-type (~15 % decrease), root elongation was much affected in *atapg9-1* (~50 % decrease).

***atapg9-1* displayed early leaf senescence ---artificially induced senescence---**

To assess the observed phenotype of *atapg9-1* in leaves were derived from loss of function of AtAPG9 in leaf cells or in other part of plant, leaf senescence in detached leaves were observed. When nutrient supply to leaves is cut off by detaching, leaf senescence is artificially induced (Oh et al., 1996). Figure 17 shows the phenotype of *atapg9-1* leaves during artificially-induced senescence. The third and fourth leaves of 3-week old plants were detached and floated on water in the continuous dark condition. Under this condition, senescence was induced in both wild-type and *atapg9-1* leaves. However, *atapg9-1* leaves turned white by day 6, while wild-type leaves remained nearly green. The observed artificially-induced senescence phenotypes was rescued by expressing a wild-type *AtAPG9* transgene in *atapg9-1* mutant plants. This result indicates that AtAPG9 functions within leaf itself to maintain cell viability.

Morphological changes of mesophyll cells during artificially-induced senescence

Microscopic analysis of leaf mesophyll cells during artificially-induced senescence was

carried out. The position of leaf segment subjected to the microscopic analysis was shown in Figure. 18A. The middle region of third or forth rosette leaves floated on the water was cut by the razor. I observed top of the mesophyll cells just beneath the epidermal cells of adaxial side. In addition to the differential interference microscope image, the fluorescence of chlorophyll was also observed. Representative images of chloroplasts in leaf mesophyll cells of wild-type plants were shown in Figure 18B-E, these images were taken after 1 day or 6 day after leaf senescence was artificially induced. As shown clearly, the shape of chloroplasts changed, from cigar-shape to round-shape and inner structure of chloroplast was gradually lost during the senescence.

Figure 19 shows the morphological changes of leaf mesophyll cells during artificially-induced senescence. In Figure 19, all images of chlorophyll fluorescence were taken in the same conditions, so basically the brightness of these images corresponds to the chlorophyll amount left in the leaves. In wild-type leaf mesophyll cells, the number of chloroplasts and the chlorophyll fluorescence in this region gradually decreased as the senescence progressed (Fig. 19A-H). However, the weak chlorophyll fluorescence was still observed from a few chloroplasts left in the leaf of 6 day after the senescence-inducing treatment (Fig. 19G and H). In *atapg9-1* leaf mesophyll cells, the decrease in chloroplast number in this region was also observed (Fig. 19I-P). However, even though the almost the same number of chloroplasts as wild-type plants were observed in 4 day after the treatment, their chlorophyll fluorescence was weaker than that of wild-type (Fig. 19F and N). At 6 day after treatment, almost all chloroplasts were lost in this region and no chlorophyll fluorescence was observed in *atapg9-1* (Fig. 19O and P). This result coincides well with the rapid senescence observed in *atapg9-1* leaves. Additionally, it seemed that chloroplasts in *atapg9-1* didn't swelled as much as in wild-type (Fig. 19E and M).

Bolting was accelerated in *atapg9-1*

I also observed the phenotype of *atapg9-1* under normal growth conditions. With a supply of typical nutrient solution, *atapg9-1* did not exhibit a significant morphological change in germination, cotyledon development, elongation of the root system and the inflorescence stem, or flowering and seed production. However, the timing of bolting was accelerated (Fig. 20A). In four independent experiments, *atapg9-1* always began bolting 2 or 3 days earlier than wild-type plants (Fig. 20B). The average rosette leaf number at the time of bolting was reduced in *atapg9-1* (9.2±0.9) compared to wild-type (11.4±1.0). These results indicate that transition from vegetative phase to reproductive phase was accelerated in *atapg9-1* mutant plants. This early bolting phenotype was rescued by expressing transgenic wild-type *AtAPG9* in *atapg9-1* plants.

In Arabidopsis, mild nitrogen starvation accelerated bolting and severe nitrogen starvation inhibited the growth of plant

The effect of nitrogen supply in the timing of inflorescence stem bolting in Arabidopsis ecotype WS was investigated. In this experiment, plants were grown under three different nitrogen supply conditions: normal nitrogen supply condition (7 mM nitrate in nutrient solution), one-tenth nitrogen supply condition (0.7 mM nitrate) and no nitrogen supply condition (0 mM nitrate). Plants were grown using rockwool and vermiculite and nitrogen was supplied as nutrient solution. As shown in Figure 21A, plant growth was clearly different depending on nitrogen conditions. In this experiment, the bolting time of plants grown under one-tenth nitrogen condition was 1 or 2 days earlier than that of plants grown under normal nitrogen condition (Fig. 21B). The average rosette leaf number at the time of bolting was reduced in plants grown under one-tenth nitrogen supply (7.5±1.1) compared to plants grown under normal nitrogen supply (9.5±1.2). However, no plants could form the inflorescence stem under no nitrogen supply condition even at 30 days after germination. In this condition, plants could produce very small 1st and 2nd rosette leaves, however, their growth seemed to be arrested in this stage (Fig. 21A). Judging from these results, mild nitrogen starvation accelerates the bolting in Arabidopsis, however, severe nitrogen starvation cause the growth arrest of the plant in early stage.

***atapg9-1* displayed early leaf senescence ---natural leaf senescence---**

I also noticed that the rosette leaves of *atapg9-1* plants senesced earlier than those of wild-type plants (Fig. 22). *atapg9-1* rosette leaves were morphologically indistinguishable from their wild-type counterparts at 17-days post-germination, but the edges of these leaves started to turn yellow in *atapg9-1* plants at day 35, while wild-type leaves were still green. Natural senescence in *atapg9-1* plants progressed in an orderly fashion from the old lower leaves to the young upper leaves as in wild-type plants.

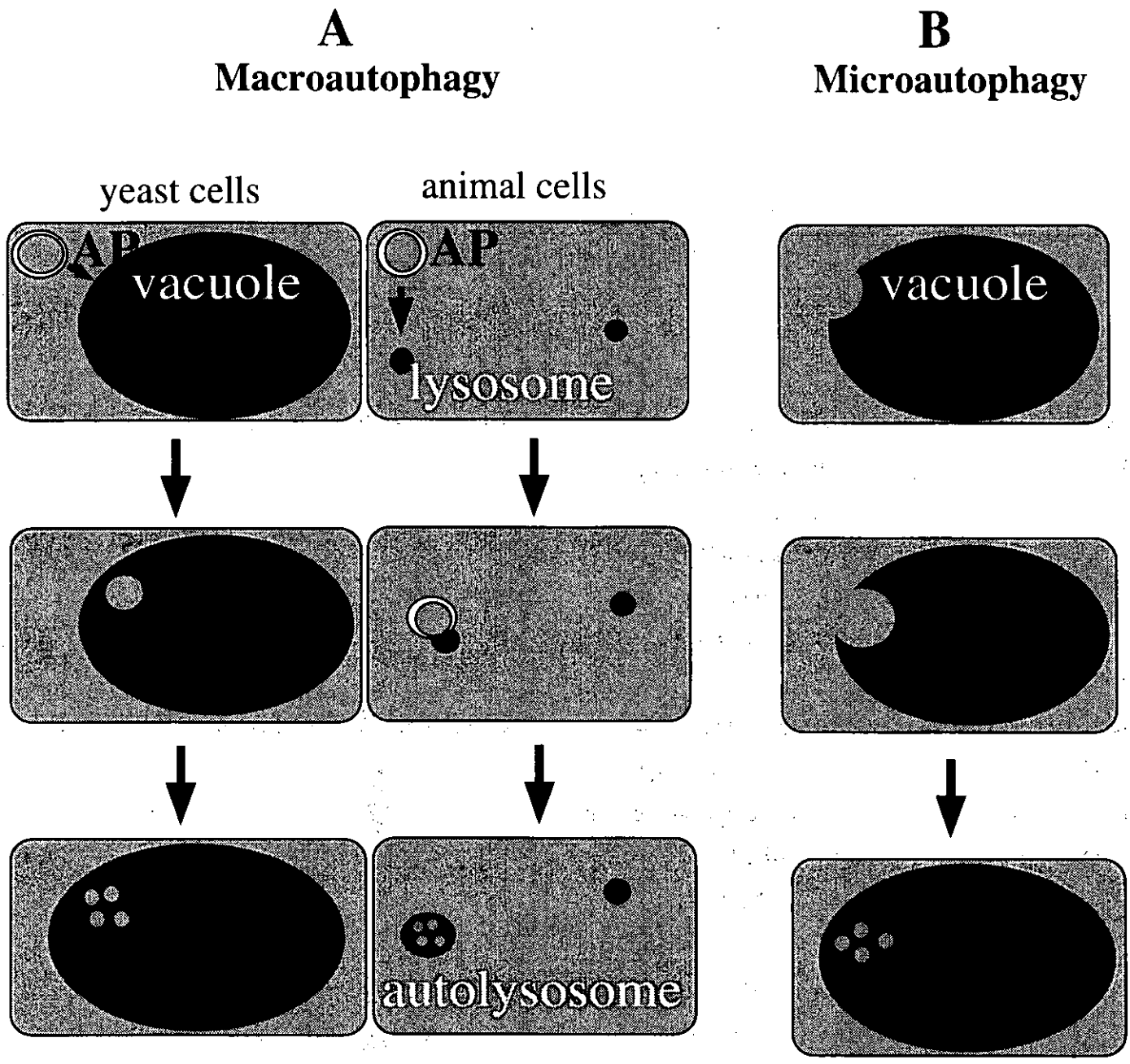

Figure 1. Model of macroautophagy and microautophagy. When cells encounter starvation conditions, a portion of cytoplasm, including organelles, is incorporated and digested in the vacuole/lysosome. This process is called autophagy and ubiquitous process throughout eukaryotes. ***A,*** Macroautophagy. 1) Cytoplasmic components are enclosed in a double membrane structure termed autophagosome (AP). 2) The outer membrane of autophagosome fuses to the vacuolar/lysosomal membrane and the inner membrane structure, autophagic body (AB), is delivered into the vacuolar/lysomal lumen. 3) The contents of autophagic body are digested by vacuolar/lysosomal proteases. ***B,*** Microautophagy. 1) The vacuolar membrane itself invaginates. 2) The vacuolar membrane enwraps the cytoplasmic components and is then pinched off. 3) The enclosed cytoplasmic contents are then degraded inside the vacuole.

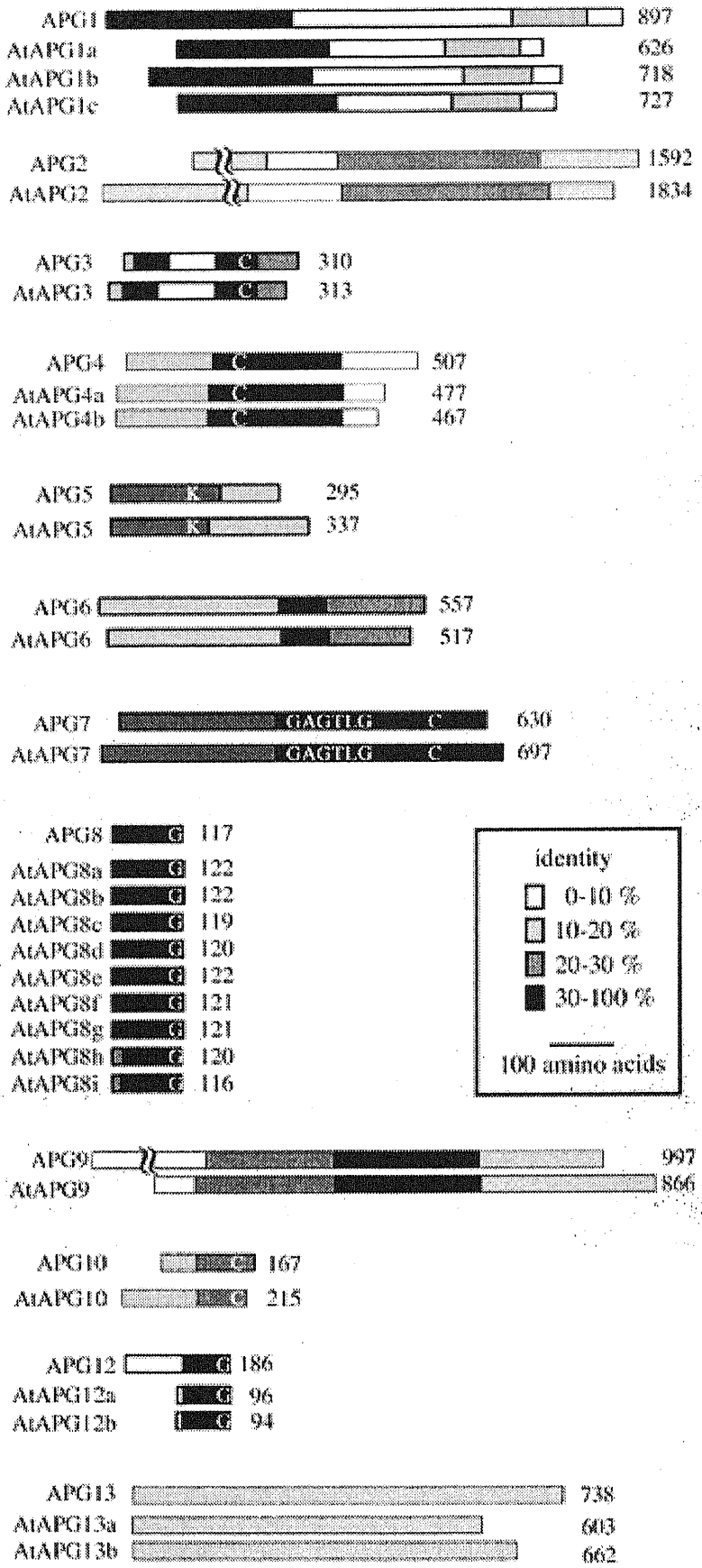

Figure 2. Comparison of yeast Apg proteins and Arabidopsis AtAPG proteins. The shading indicates the degree of identity between each homologous region. Each protein was aligned based on the CLUSTAL V method using DNASTAR. Conserved amino acid residues important for proper Apg function are indicated by letters. The numbers indicate the amino acid length of each protein.

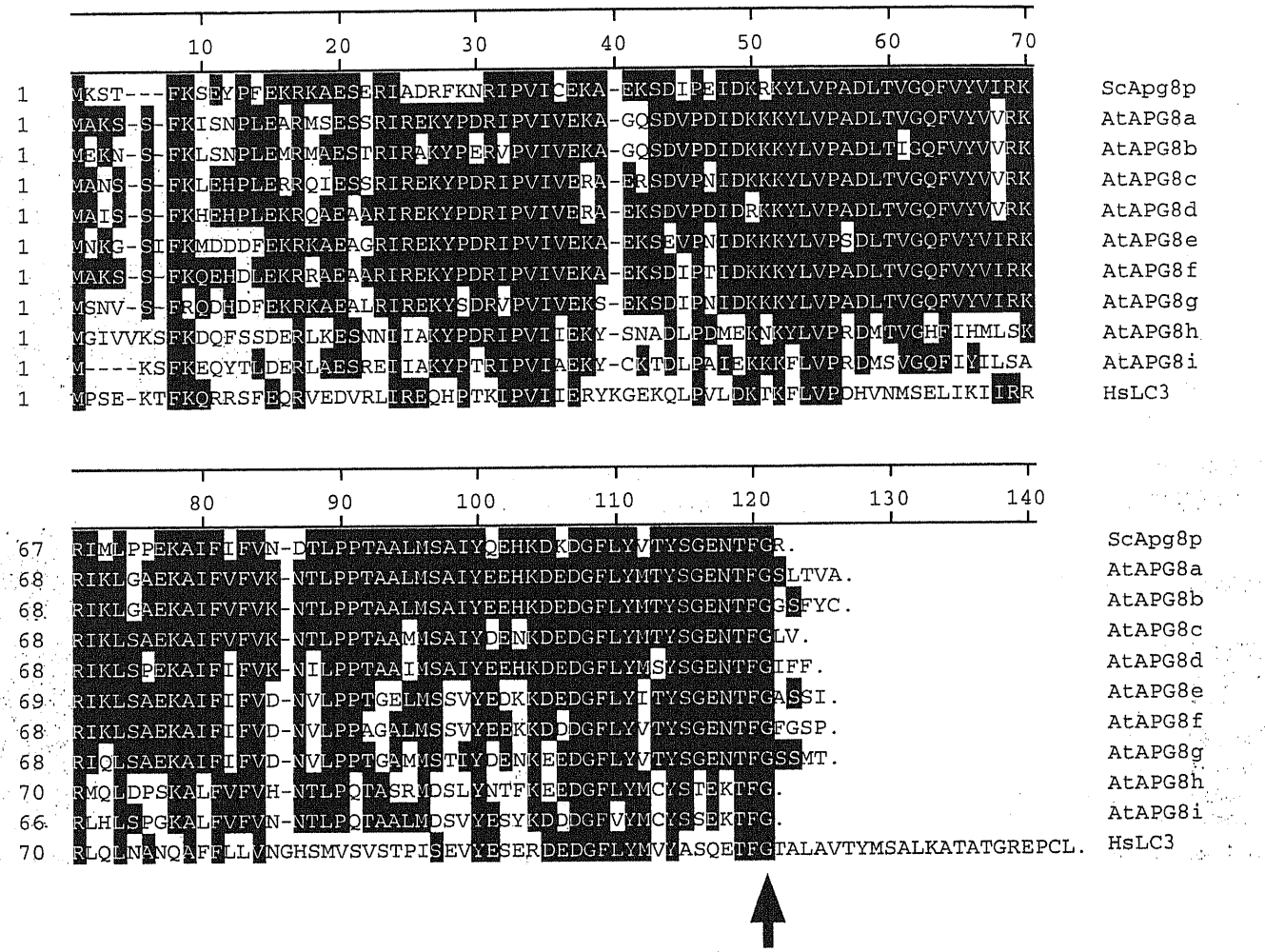

Figure 3. Alignment of amino acid sequences of AtAPG8 proteins and its homologs. Each protein was aligned by the CLUSTAL V method using DNASTAR. Arrow indicates an invariant glycine residue, which corresponds to Gly 116 of ScApg8p that exposes at the carboxy-teminus by cleavage by ScApg4p. Residues that match the consensus are shaded in black. At, *Arabidopsis thaliana*; Sc, *Saccharomyces cerevisiae*; Hs, *Homo sapiens*. ScApg8p (Kirisako et al., 2000), HsLC3 (Kabeya et al., 2000).

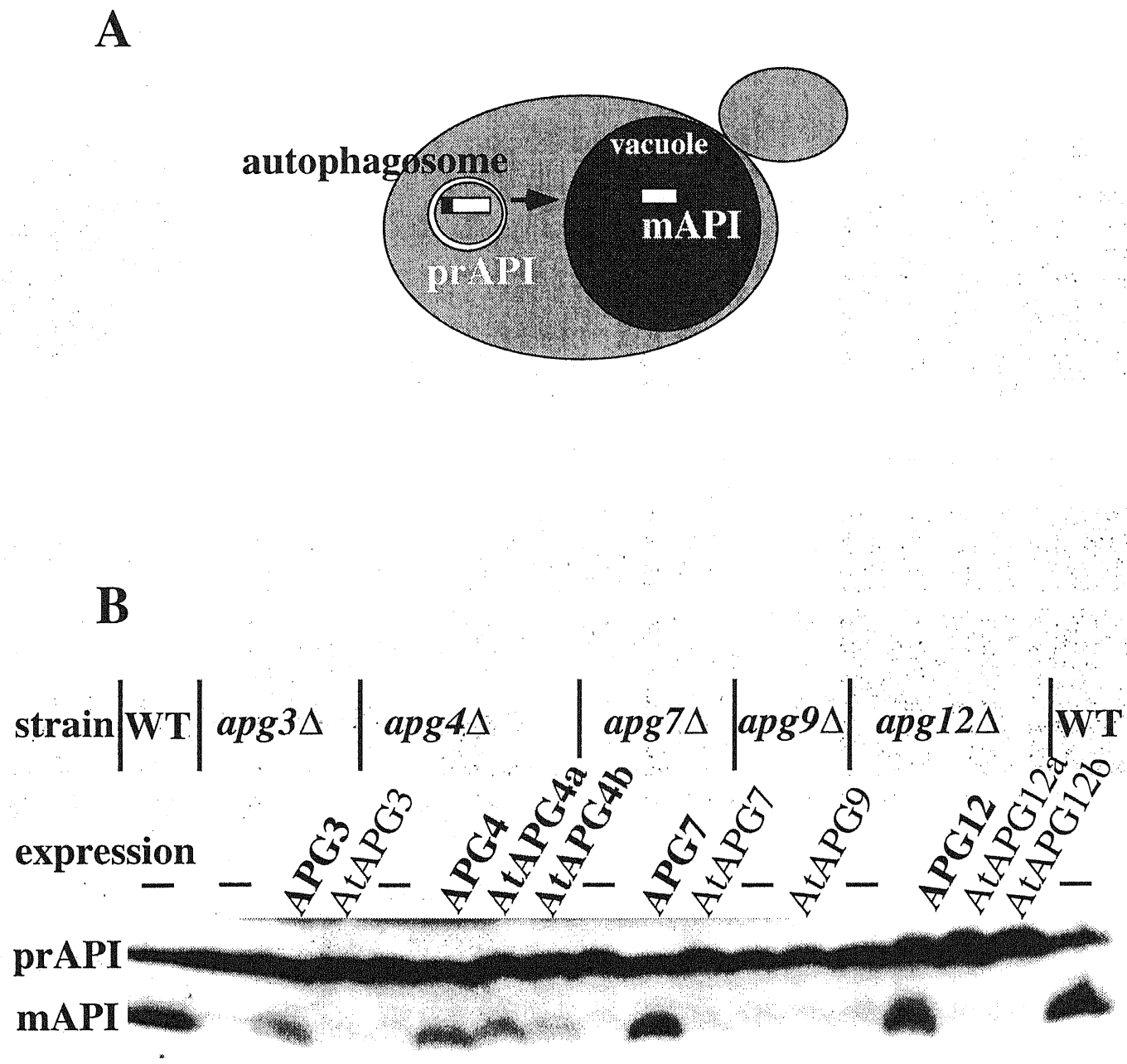

Figure 4. Complementation analysis of yeast *apg* mutants. ***A*** **,** Model of API maturaion. prAPI is synthesized in the cytosol, then transported to the vacuole by autophagy during starvation. In vacuole, prAPI is processed to form mAPI. Thus, autophagy can be monitored as maturation of API. ***B*****,** The result of complementation test. The coding sequences of AtAPG proteins were cloned into a yeast expression vector. Protein extracts were analyzed by immunoblot using antiserum to API. The positions of precursor and mature API are indicated. The defect of maturation of prAPI in *Δapg4* cells were comlemented by both AtAPG4a and 4b, as indicated by the presence of vacuolar mAPI.

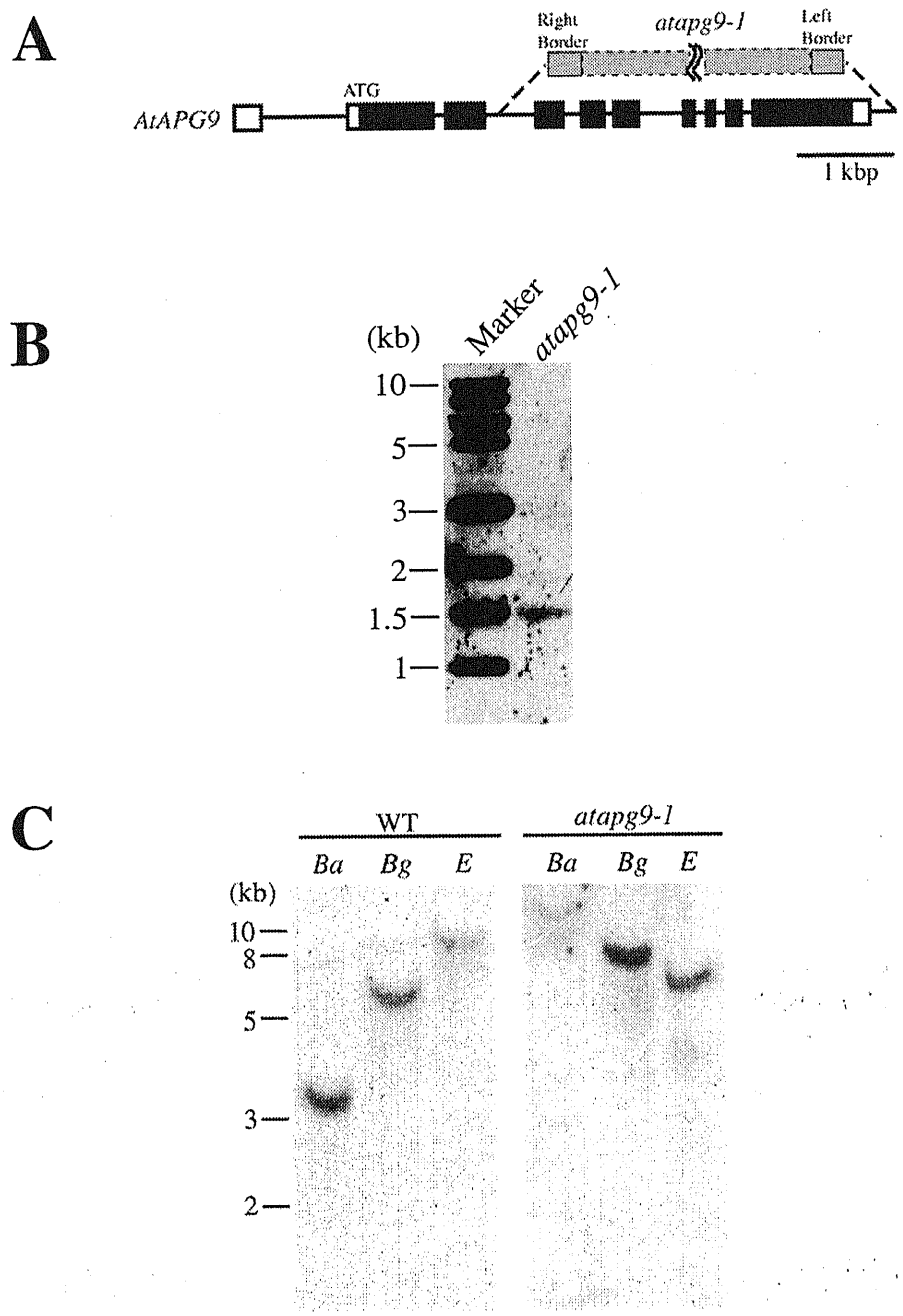

Figure 5. Identification of the T-DNA insertional *AtAPG9* knockout mutant *atapg9-1*. *A,* Genomic structure of the *AtAPG9* gene. Lines indicate introns and boxes indicate exons; white boxes, untranslated regions; black boxes, translated regions. The T-DNA insertion site in the *atapg9-1* allele is indicated by the grey box. ***B,*** Southern blot analysis of the T-DNA insertional sequences. Arabidopsis genomic DNA from *atapg9-1* mutant plants was digested with *Bam*HI and the blot was hybridized with a cauliflower mosaic virus 35S promoter probe. ***C,*** Southern blot analysis of the *AtAPG9* gene. Arabidopsis genomic DNA from wild-type (WT) and *atapg9-1* mutant plants was digested with *Bam*HI (Ba), *Bgl*II (Bg), or *Eco*RV (E) and the blot was hybridized with an *AtAPG9* probe.

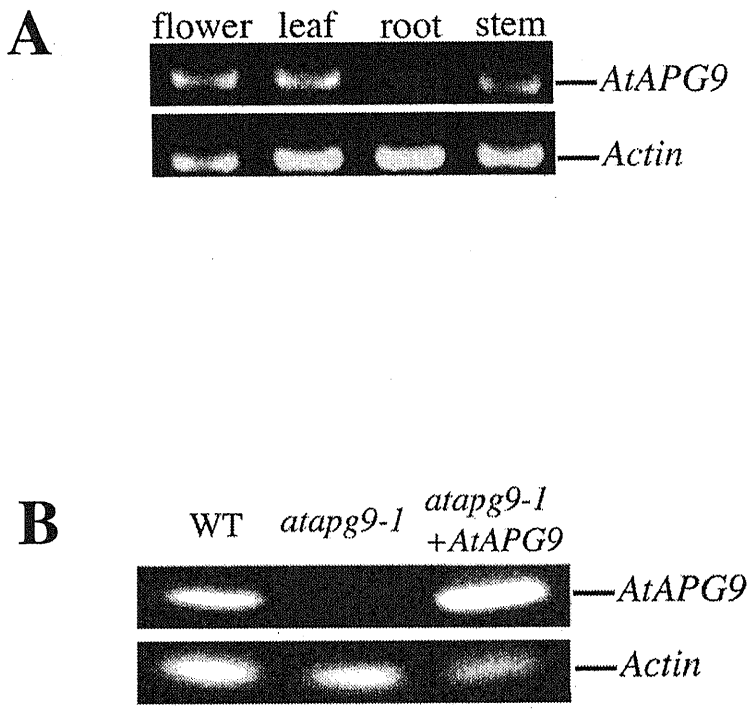

Figure 6. Expression of *AtAPG9*. *A,* RT-PCR analysis of *AtAPG9* expression in various organs. Total RNA was isolated from flowers, leaves, stems and roots of wild-type plants grown hydroponically for 1 month. RT-PCR was performed using gene-specific primers for *AtAPG9* and for actin *ACT2* gene. After agarose electrophoresis, the gel was stained with ethidium bromide. ***B,*** RT-PCR analysis of the *AtAPG9* gene. Total RNA was isolated from the aerial parts of wild-type and *atapg9-1* plants, and from *atapg9-1* plants transformed with the wild-type *AtAPG9* gene. RT-PCR was performed using gene-specific primers for *AtAPG9* and for the actin gene *ACT2*. After agarose electrophoresis, the gel was stained with ethidium bromide.

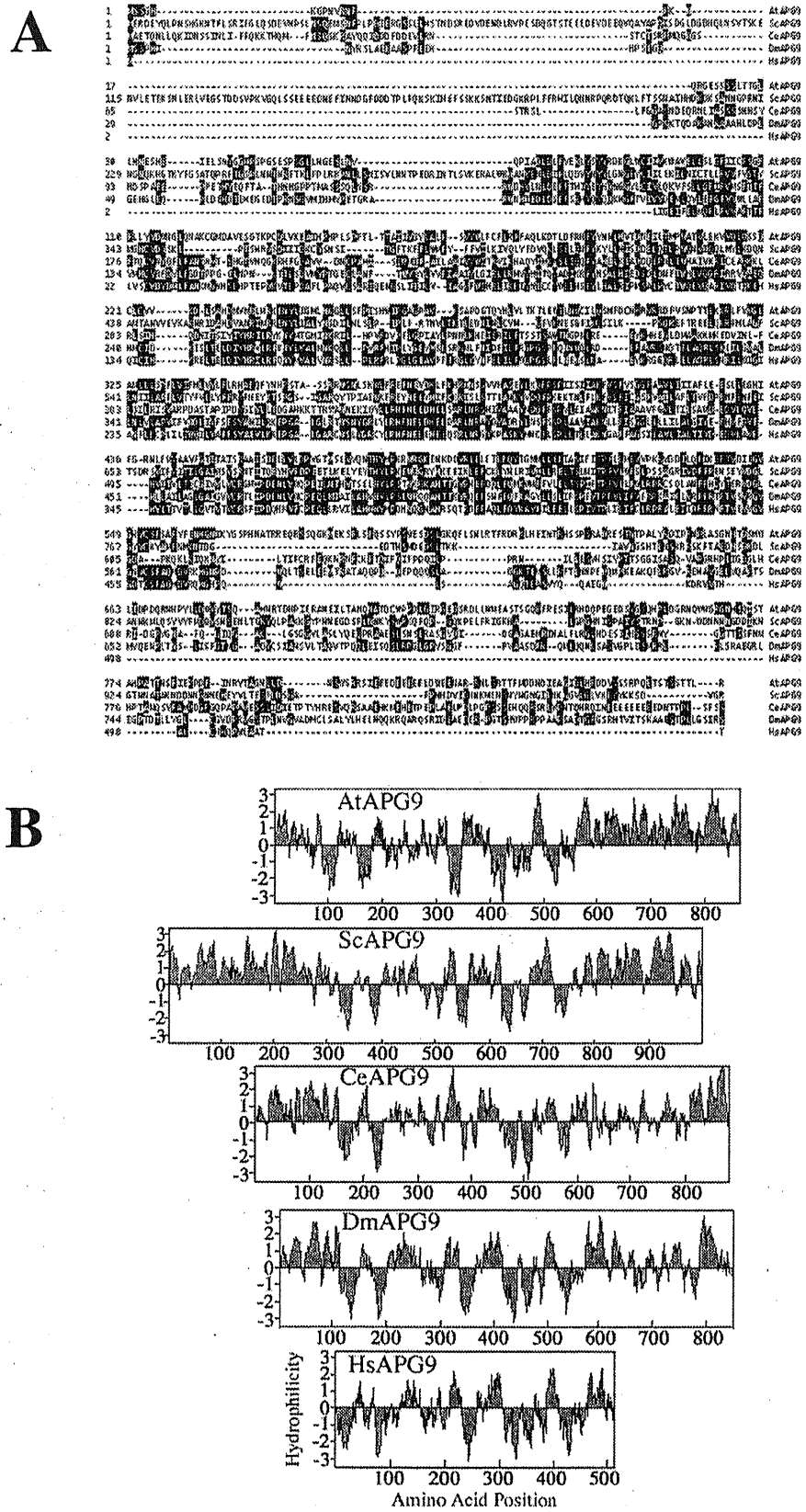

Figure 7. Comparison of APG9 homologs. Each protein was aligned by the CLUSTAL V method using DNASTAR. ***A,*** Amino acid alignment of AtAPG9 and its homologs. Residues that match the consensus are shaded in black. At, *Arabidopsis thaliana*; Sc, *Saccharomyces cerevisiae*; Ce, *Caenorhabditis elegans*; Dm, *Drosphila melanogaster*; Hs, *Homo sapiens*. ***B,*** Comparison of hydrophilicity plots of AtAPG9 and its homologs. Based on the Kyte-Doolittle algorithm (Kyte and Doolittle, 1982), AtAPG9 is predicted to have 5 to 7 transmembrane domains.

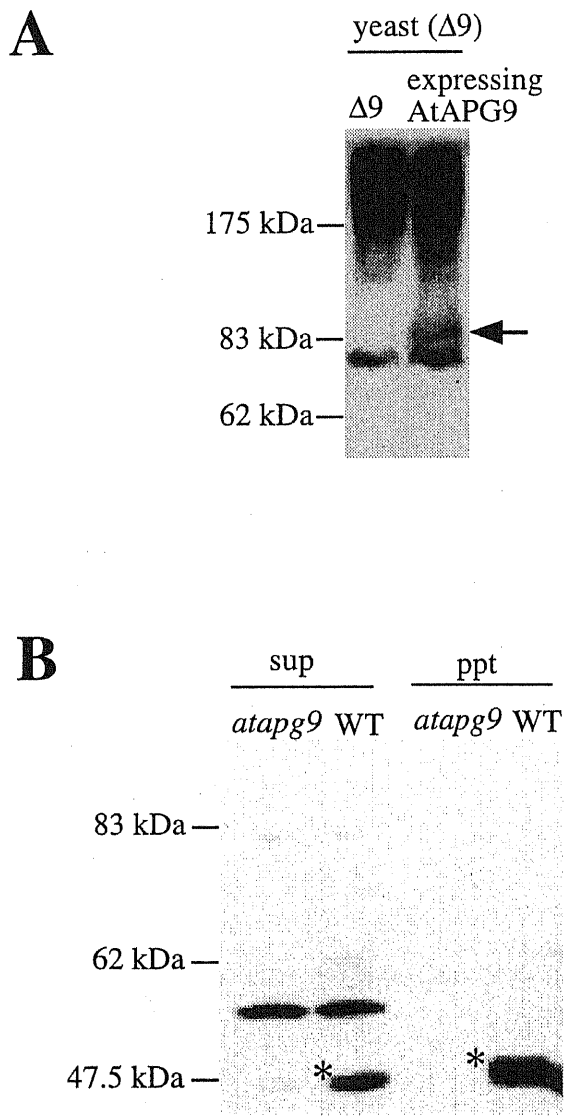

Figure 8. Immunoblotting of AtAPG9. ***A,*** Immunoblotting of AtAPG9 using yeast lysates. Yeast total lysates were prepared from yeast Δ*apg9* cells and Δ*apg9* cells expressing AtAPG9 as described in Materials and Methods. The putative AtAPG9 (predicted MW=99kDa) is indicated by the arrow. ***B,*** Immunoblot using plant lysates. Lysates prepared from wild-type plants (WT) and *atapg9-1* mutant plants were subjected to the immunoblot using affinity purified anti-AtAPG9. Total plant lysates were centrifuged at 100,000 g for 1 h to generate supernatants (sup) and pellets (ppt). The putative AtAPG9 degradation products are marked by the asterisks.

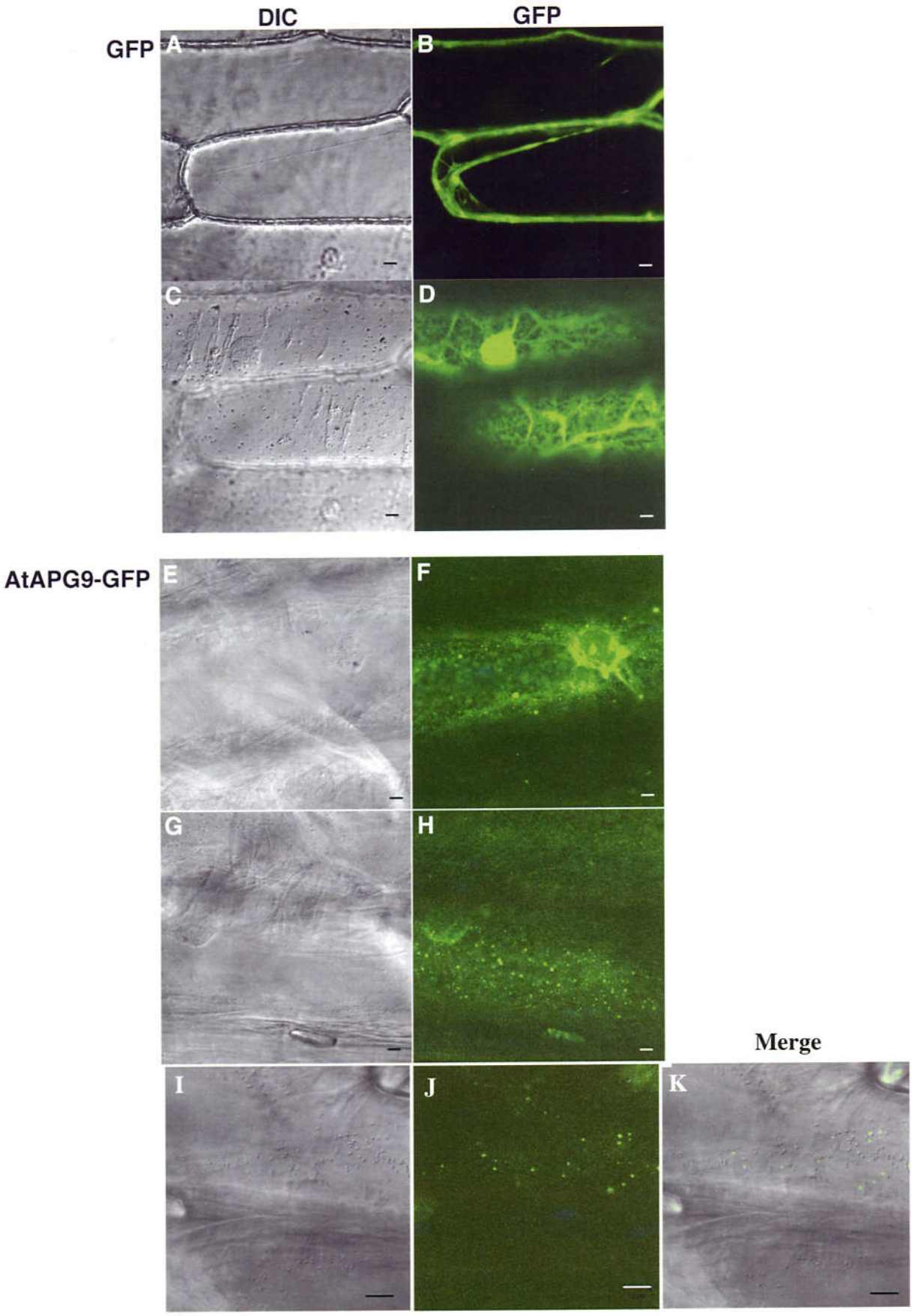

Figure 9. Localization of AtAPG9-GFP. (***A-D***) Localization of GFP in onion epidermal cells. GFP are expressed from cauliflower mosaic virus 35S promoter. (A and C) Differential interference microscope images (DIC). (B and D) Fluorescence images of GFP. (***E-K***) Localization of AtAPG9-GFP in onion epidermal cells. AtAPG9-GFP are expressed from cauliflower mosaic virus 35S promoter. (E, G and I) DIC images. (F, H and J) Fluorescence images of AtAPG9-GFP. (K) Merged image of DIC image and fluorescent image.

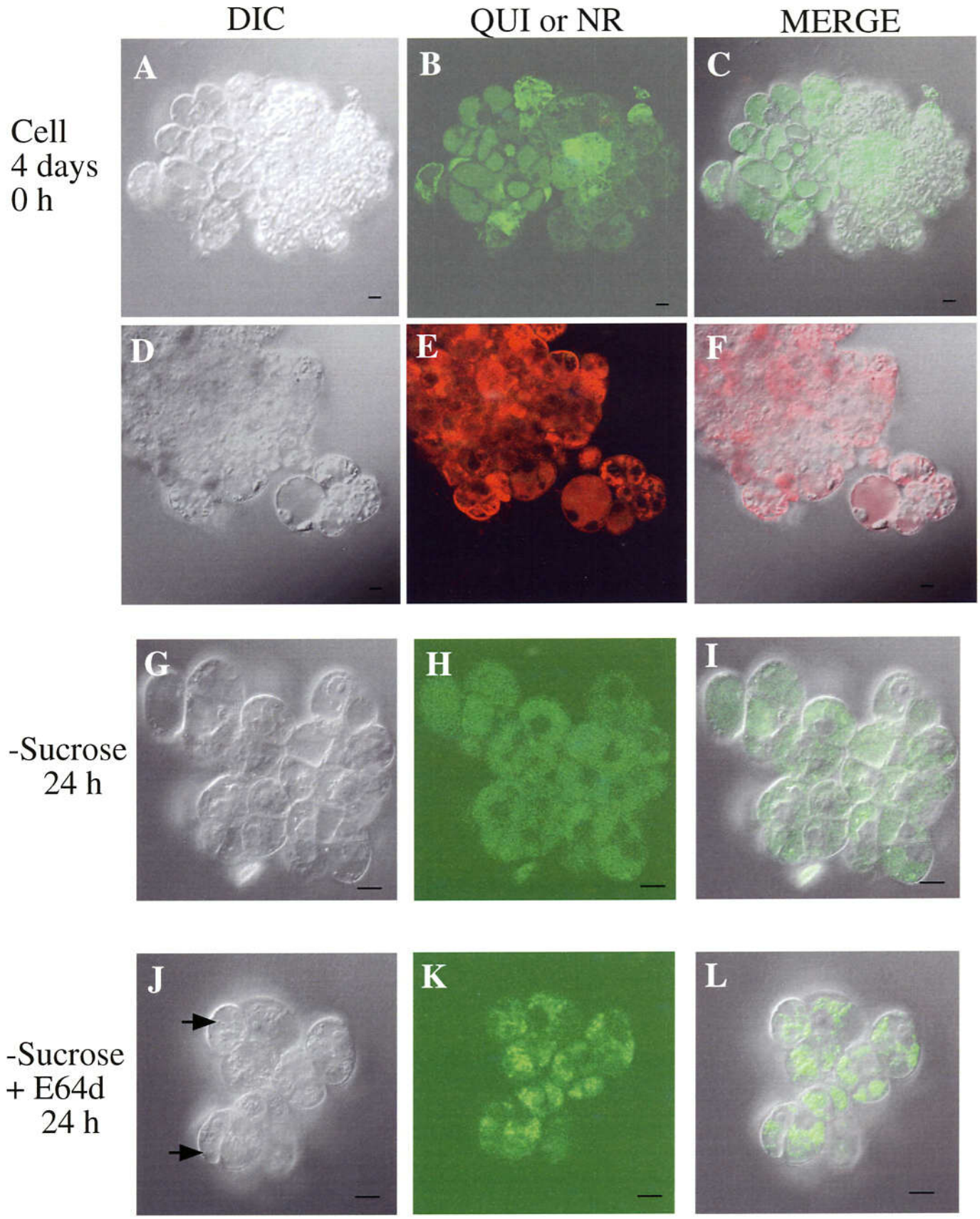

Figure 10. Morphological changes of the Arabidopsis suspension-cultured cells during sucrose starvation. Cells were stained with 40 μM quinacrine (QUI: green) or 35 μM neutral red (NR:red). (***A-F***) The cells before starvation, (***G-I***) the cells after sucrose starvation treated with 0.1% DMSO for 24 hrs, (***J-L***) the cells after sucrose starvation treated with 10 μM E64d for 24 hrs. (A, D, G and J) DIC images, (B, E, H and K) Fluorescent images of acidtropic dyes, (C, F, I and L) Merged images of DIC images and fluorescent images. Sperical bodies in motion are indicated by arrows. Bar: 10 μm.

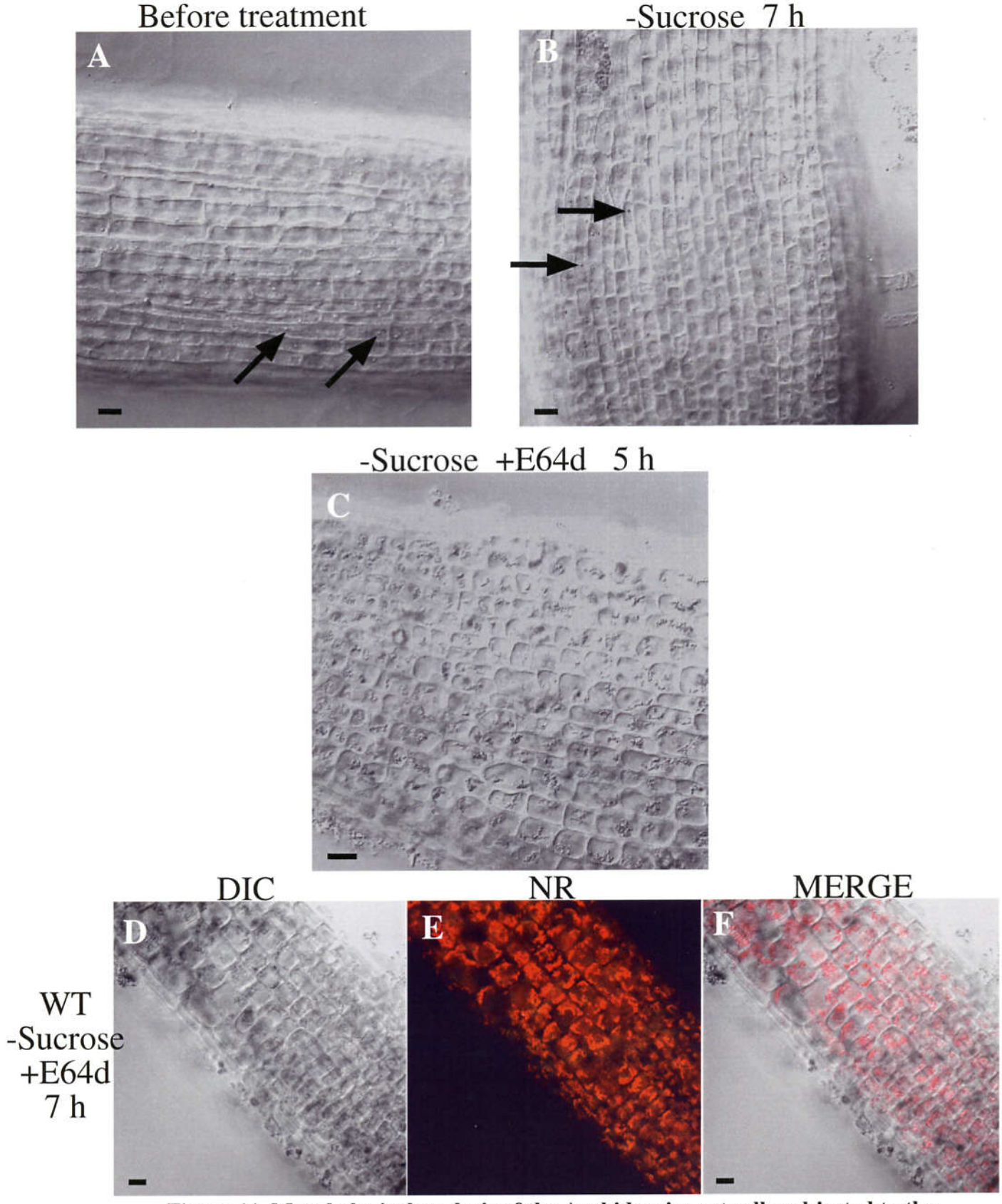

Figure 11. Morphological analysis of the Arabidopsis root cells subjected to the sucrose starvation. ***A,*** Wild-type root cells before starvation. ***B,*** Wild-type root cells after starvation treated with 0.1% DMSO for 7 hrs. ***C,*** Wild-type root cells after starvation treated with 10 μM E64d for 5 hrs. ***D-F,*** Wild-type root cells after starvation treated with 10 μM E64d for 7 hrs. The cells were stained with 35 μM neutral red (NR:red). Arrows indicate particles observed in the central vacuole. (A-D) DIC images, (E) Fluorescent images of NR, (F) Merged images of DIC images and fluorescent images. Bar: 10 μm.

wild-type
-Sucrose
+E64d
7 h

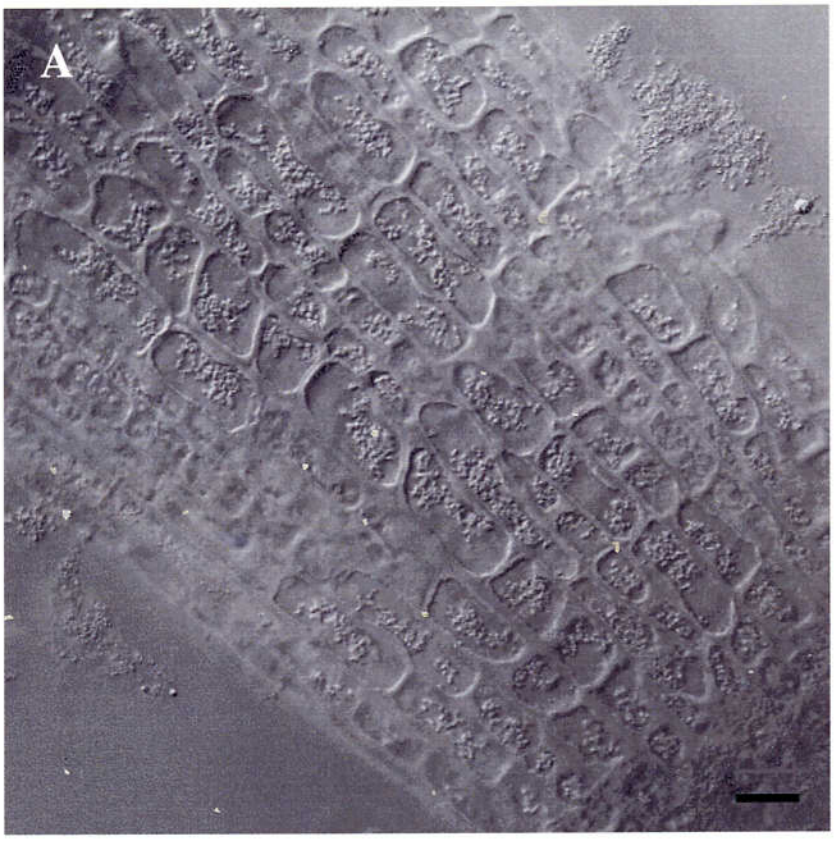

atapg9-1
-Sucrose
+E64d
7 h

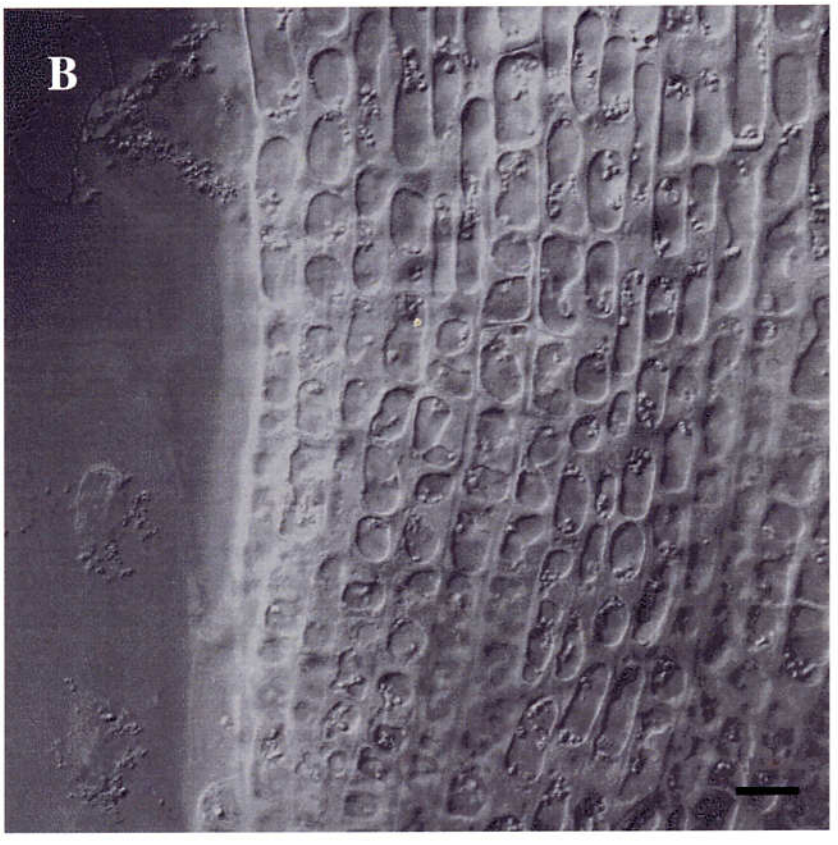

Figure 12. Comparison of accumulation of spherical bodies in wild-type and *atapg9-1* root cells. ***A,*** Wild-type root cells after starvation treated with 10 μM E64d for 7 hrs. ***B,*** *atapg9-1* root cells after starvation treated with 10 μM E64d for 7 hrs. Bar: 10 μm.

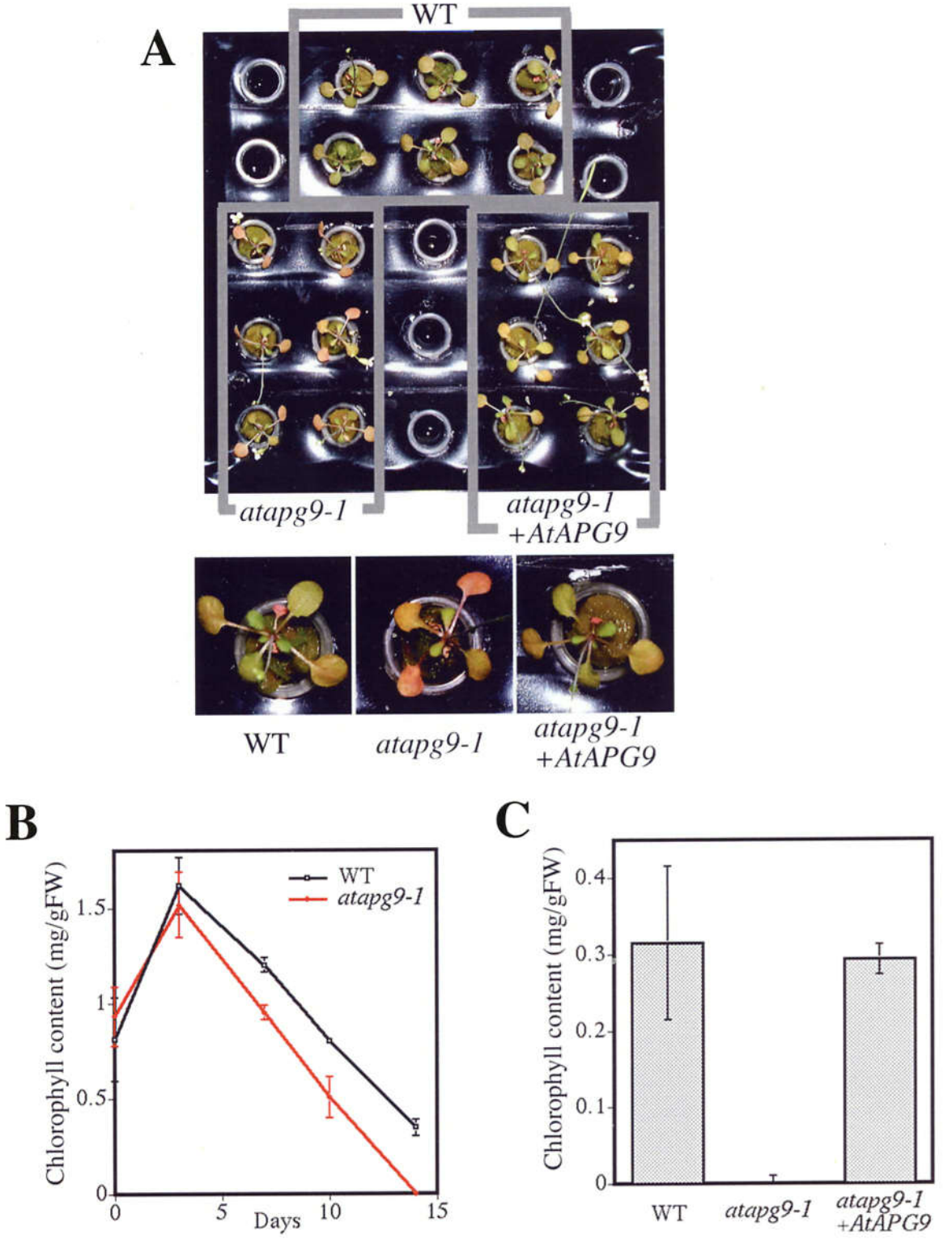

Figure 13. AtAPG9 suppressed nitrogen starvation-induced chlorosis. ***A,*** Top view of 24-day-old nitrogen-starved plants. Plants were grown with nutrient medium containing 7 mM nitrate for 10 days, then transferred to nitrogen-depleted (0 mM nitrate) medium and grown hydroponically for 14 days. ***B,*** Time course analysis of chlorophyll content. Chlorophyll was extracted from the 1st and 2nd rosette leaves at the day indicated after induction of nitrogen starvation. ***C,*** Complementation of the *atapg9-1* phenotype. Chlorophyll was extracted from the 1st and 2nd rosette leaves of plants grown for 14 days under nitrogen starvation condition. All measurements were made on at least 3 individual plants.

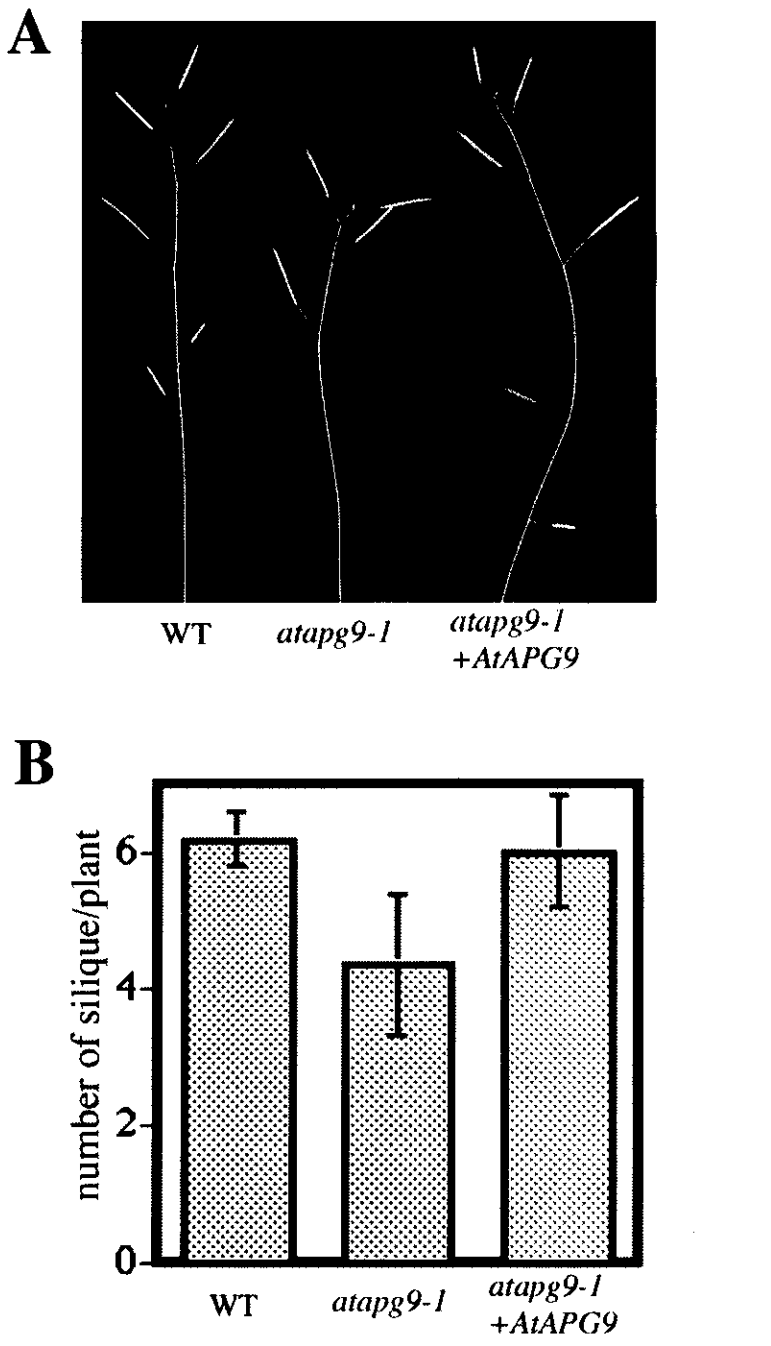

Figure 14. AtAPG9 was required for efficient seed production under nitrogen starvation conditions. ***A,*** Representative 2-month old plants grown hydroponically under nitrogen starvation conditions. ***B,*** Number of siliques produced per plant grown under nitrogen starvation conditions for 2 months. All measurements were made on at least 4 individual plants.

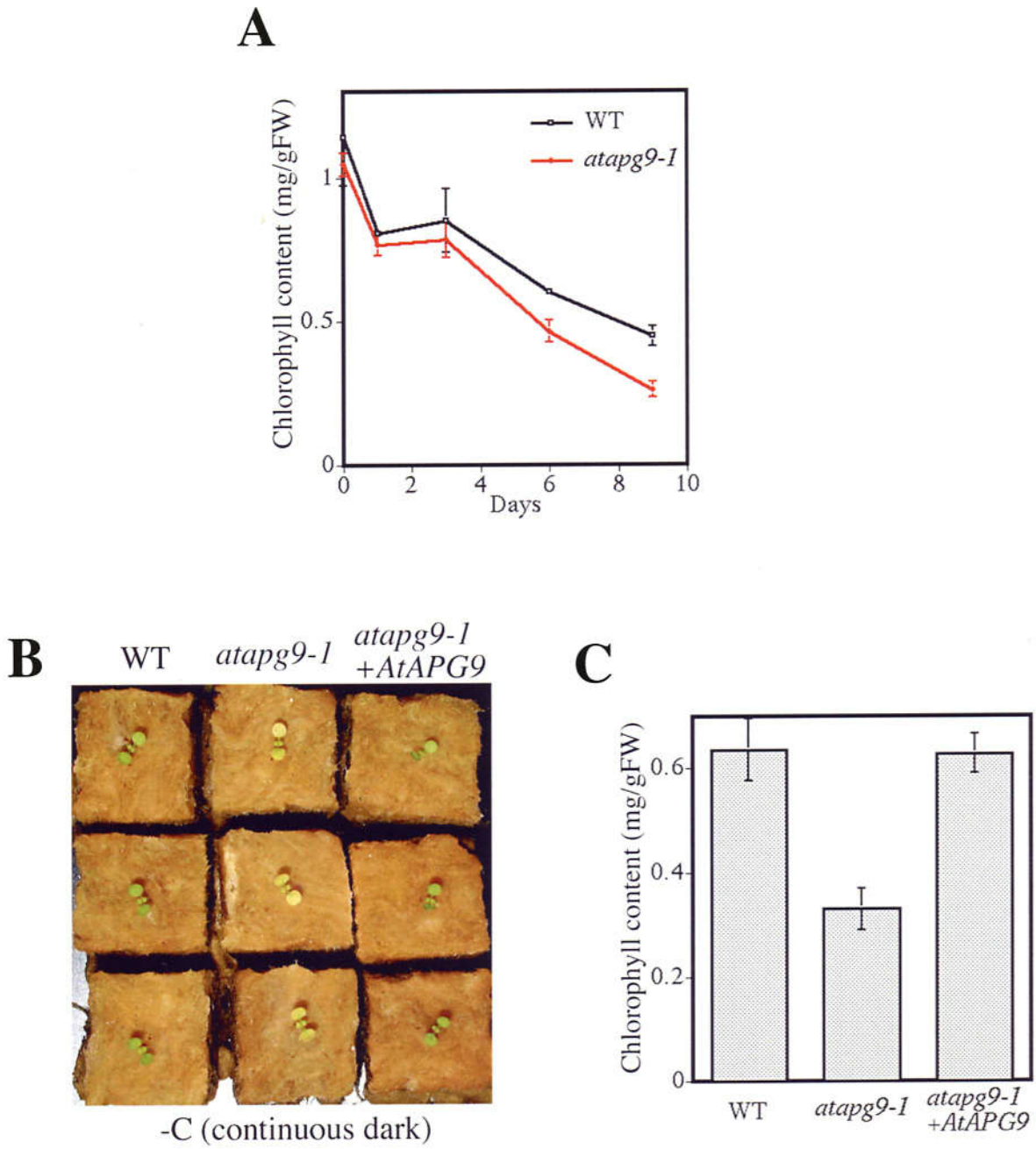

Figure 15. AtAPG9 suppressed carbon starvation-induced chlorosis. ***A,*** Time course analysis of chlorophyll content. Plants were grown for 7 days with a light cycle of 16 h light/8 h dark, after which they were maintained in the dark. Chlorophyll was extracted from 2 cotyledons at the day indicated after transfer to continuous dark conditions. ***B,*** Top view of 15-day-old carbon-starved plants. Plants were photographed after 8 days of carbon starvation. ***C,*** Complementation of the *atapg9-1* phenotype. Chlorophyll was extracted from 2 cotyledons of plants grown for 8 days under carbon starvation conditions. All measurements were made on at least 3 individual plants.

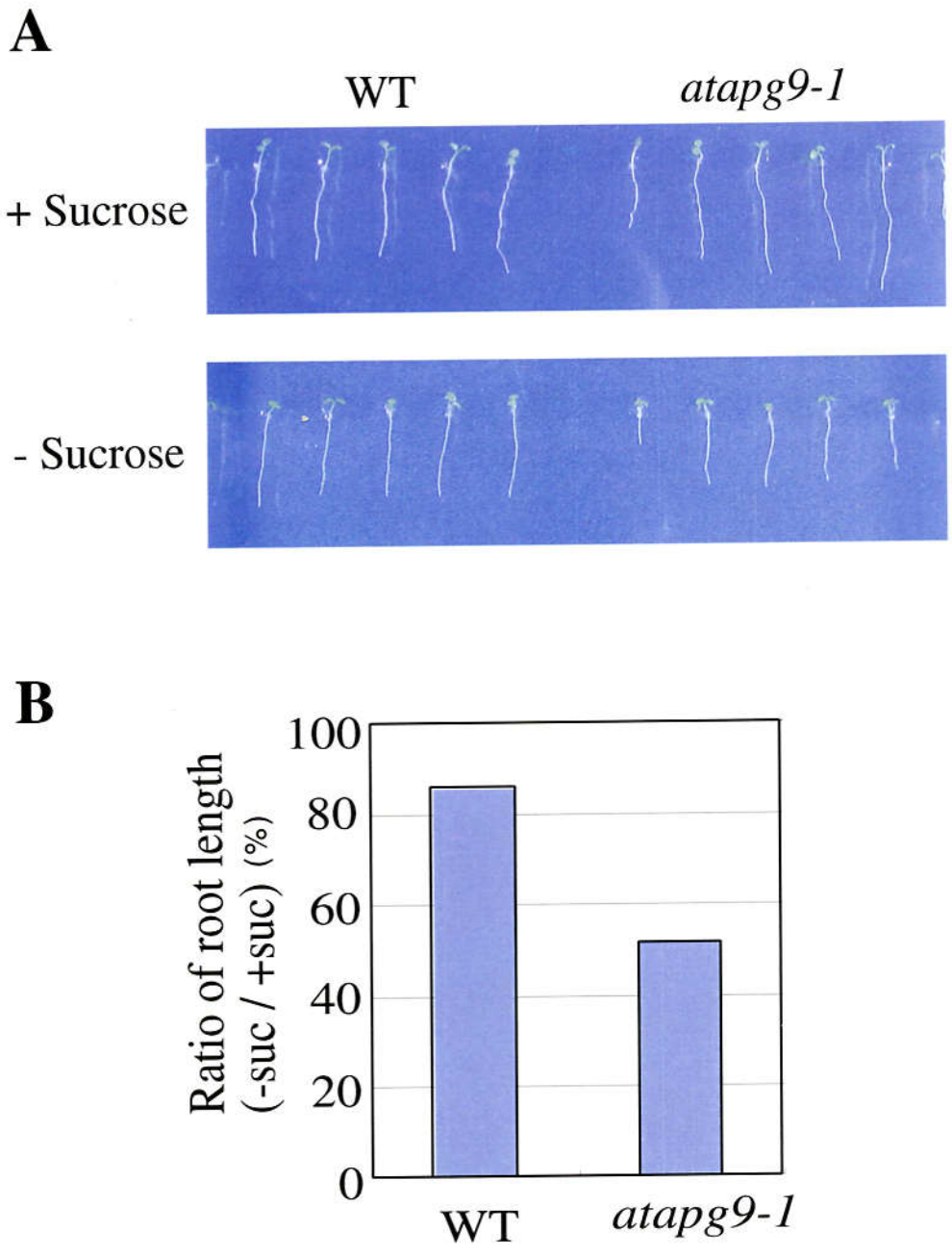

Figure 16. Root elongation was affected by sucrose starvation in *atapg9-1*. *A*, Photogaraphs of seedling at 4 days after germination. Wild-type and *atapg9-1* plants were grown on the vertical plate of 1/2 MS medium with or without sucrose for 4 days. ***B*,** Ratio of the root length on the sucrose depleted medium to the root length on the sucrose containing medium. The average root length on each condition was compared. Measurements were made on at least 12 individual plants.

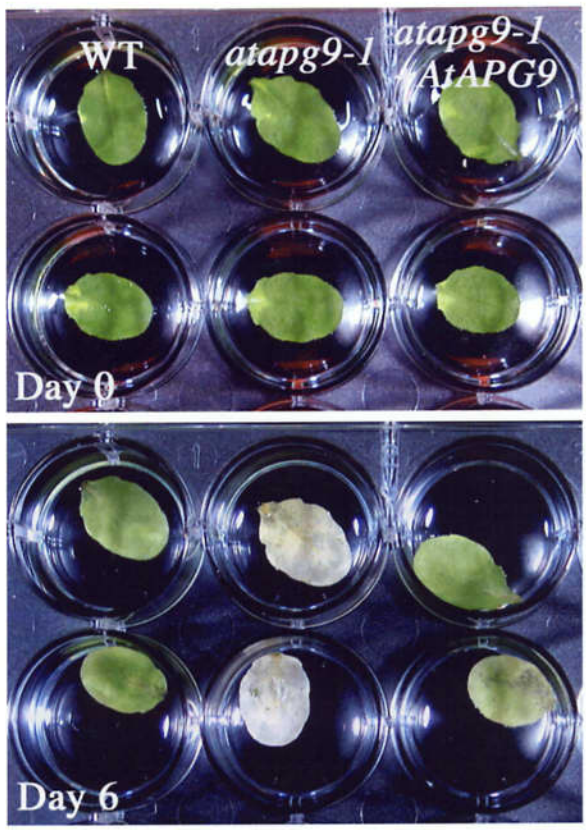

Figure 17. AtAPG9 was involved in regulation of leaf senescence. Artificially induced senescence of detached leaves. The third or fourth rosette leaves of 3-week old plants were detached and floated on water. The leaves were incubated at 22 °C in the dark and photographed at day 0 and after 6-day incubation.

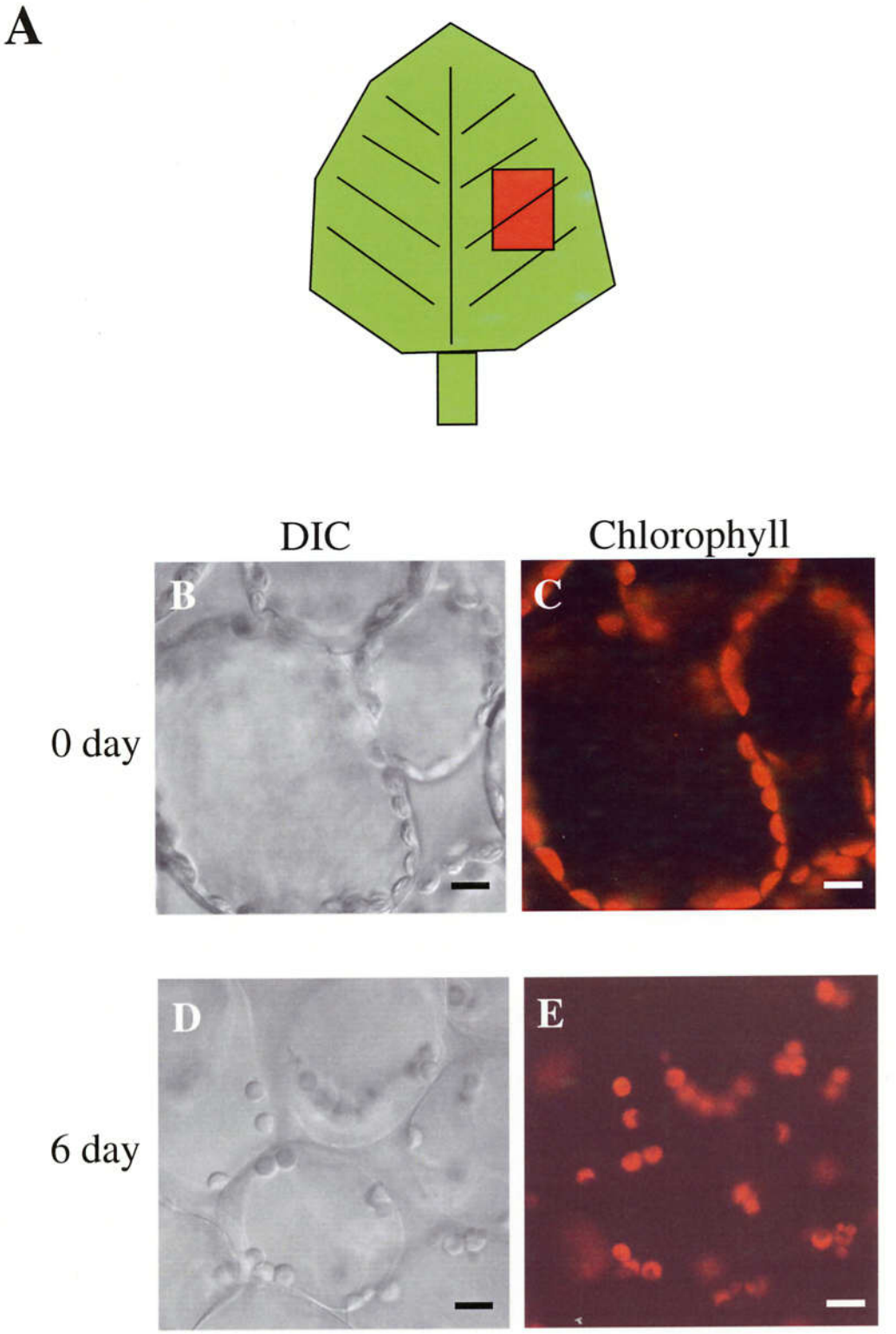

Figure 18. Morphological changes of the chloroplasts during artificially-induced senescence. ***A,*** Representative image of leaf sample location. Area coloured in red was subjected to the microscopic analysis. ***B and C,*** The leaf mesophyll cells of wild type plants at 0 day after floatation on the water. ***D and E,*** The leaf mesophyll cells of wild-type plants at 6 day after floatation on the water. (A and C) DIC images, (B and D) the fluorescent images of chlorophyll. Bar: 10 μm.

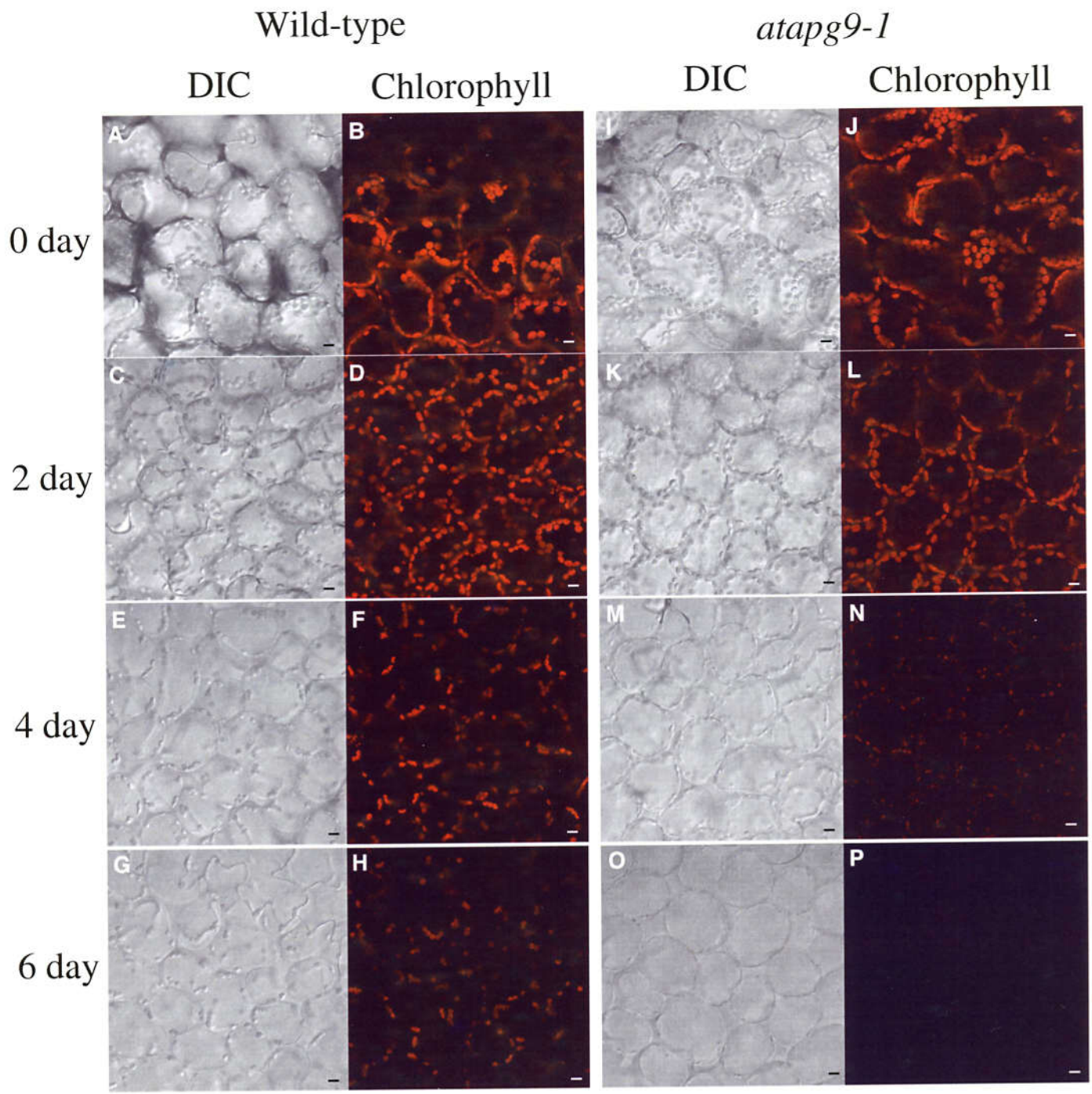

Figure 19. Morphological changes of the Arabidopsis leaf mesophyll cells during artificially-induced senescence. ***A-H,*** The leaf mesophyll cells of wild type plants. ***I-P,*** the leaf mesophyll cells of *atapg9-1* plants. Photos were taken at days as indicated after the 3rd and 4th rosette leaves were floated on the water. (A, C, E, G, I, K, M and O) DIC images, (B, D, F, H, J, L, N and P) the fluorescent images of chlorophyll. Bar: 10 μm.

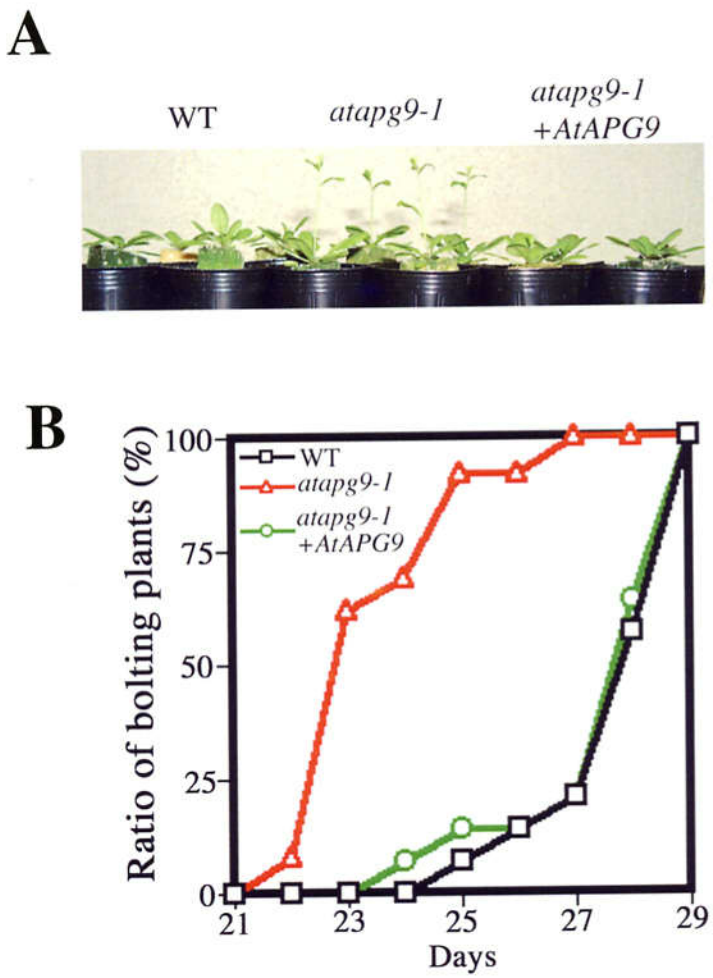

Figure 20. The onset of bolting was accelerated in *atapg9-1* plant. ***A,*** Side view of 26-day-old plants. Wild-type and *atapg9- 1* plants were grown at 22 °C with a 16 h light/8 h dark cycle supplied with standard nutrient solution. ***B,*** Time course analysis of inflorescence stem bolting. The number of plants containing at least one primary inflorescence stem longer than 5 mm was counted daily. All measurements were made on at least 13 individual plants.

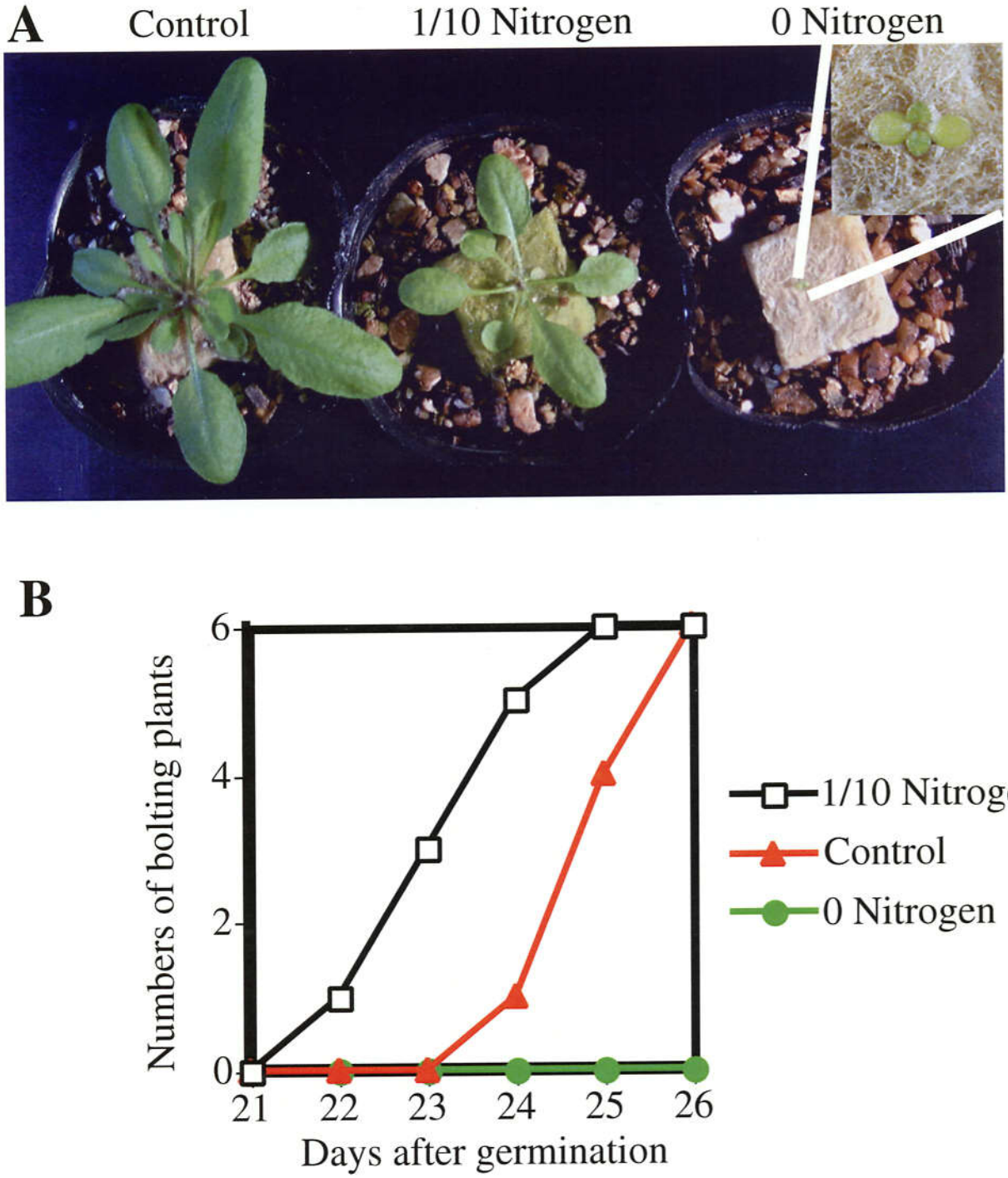

Figure 21. The onset of bolting was accelerated by slight nitrogen starvation in Arabidopsis. ***A,*** The representative image of plants grown under 3 different nitrogen supply conditions. ***B,*** Time course analysis of inflorescence stem bolting. The number of plants containing at least one primary inflorescence stem longer than 5 mm was counted daily. All measurements were made on 6 individual plants.

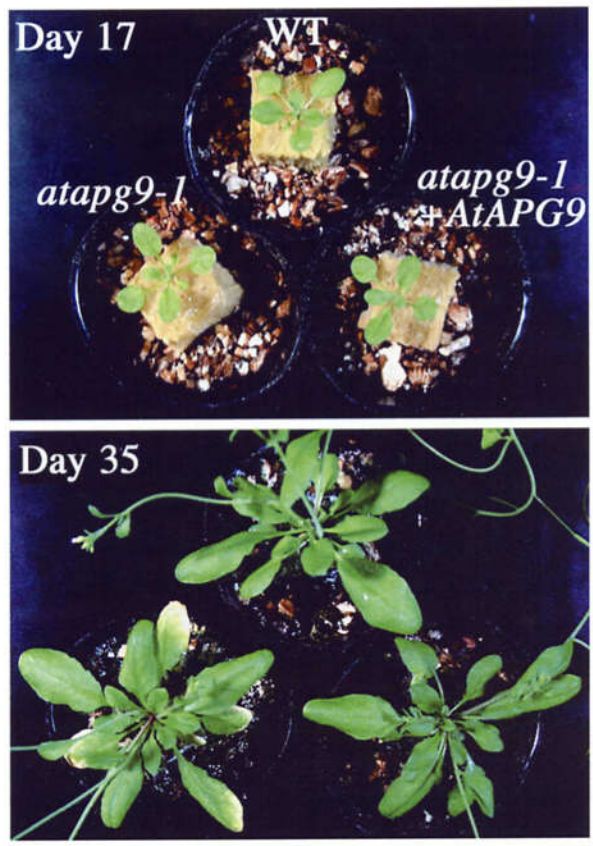

Figure 22. Natural leaf senescence was accelerated in *atapg9-1*. Wild-type, *atapg9-1* and *atapg9-1* transformed with wild-type *AtAPG9* gene were grown under standard conditions and photographed on day 17 and 35 after germination.

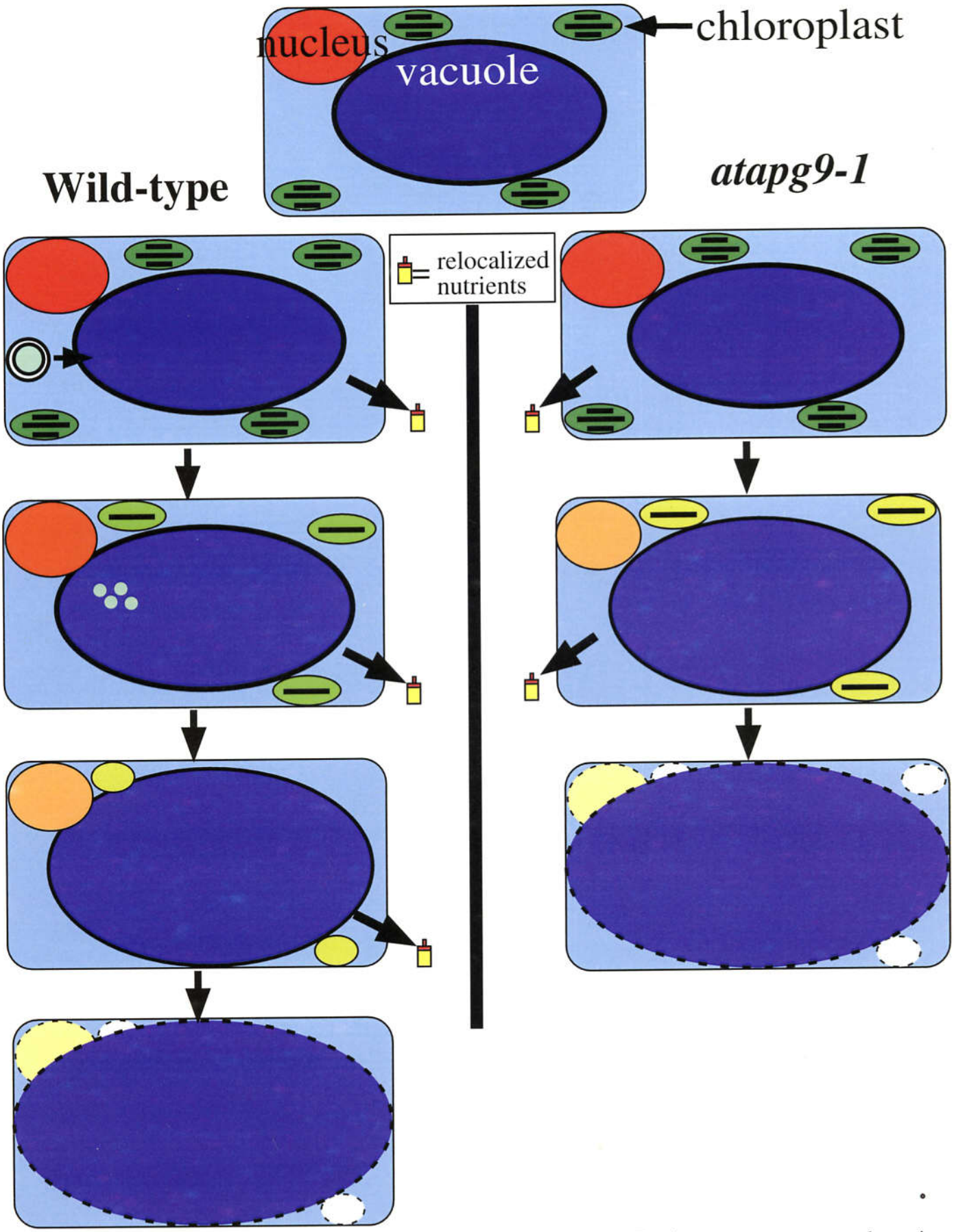

Figure 23. Model of leaf senescence in wild-type and *atapg9-1*. During senescence, autophagy is induced and the degradation products are reused as nutrient sorces for the maintenance of cell viabillity, With this system, cells can degrade themselves gradually and nutrients are re-localized efficiently. However, in *atapg9-1*, the defect in autophagy cause more rapid cell death and because of it, the efficient relocalization of nutrients is inhibited. In this model, wild-type cell can relocalize 3 units of nutrients until cell death is completed, however *atapg9-1* cell can relocalize only 2 unit of nutrients until cell death is completed.

Discussion

APG genes are well conserved in plant

This study revealed that most of yeast *APG* gene homologs exist in Arabidopsis genome. Of the total 15 *APG* genes that encode proteins necessary for yeast autophagy, 12 of them were found to have at least one homologous counterpart in Arabidopsis (Fig. 2). Because the functional domains and essential amino acid sequences of the resulting AtAPG proteins are well-conserved between yeast and plants, it seems likely that their biological functions are also well-conserved. Indeed, I confirmed that both *AtAPG4a* and *AtAPG4b* could complement the autophagic defect of the yeast *apg4* mutation (Fig. 4). Based on these facts, it is reasonable to deduce that the AtAPG proteins are involved in autophagy in plant cells. A part of this assumption has been proven in mammalian cells, as several mammalian APG proteins have been shown to be essential for autophagy (Liang et al., 1999; Mizushima et al., 2001), and to act via a molecular mechanism quite similar to that of yeast (Kabeya et al., 2000; Mizushima et al., 1998b; Tanida et al., 2001).

Multiplication of *APG* gene in Arabidopsis

Yeast cells have single paralog of respective *APG* genes. However, it turns out that Arabidopsis possesses a multiple paralog of several *APG* genes. To our surprise, there are nine Apg8 homologs in Arabidopsis (Fig. 2). This may indicate that several types of autophagy are used properly according to each organ and state of development. The organ specific band pattern observed in immunoblotting of AtAPG8 using antibody against yeast Apg8p suggests that AtAPG8 molecules are kept in different state to perform the distinct biological function according to organs (data not shown). Especially, two of nine homologs, AtAPG8h and AtAPG8i, do not possess an extra amino acid tail downstream of the conserved Gly (Fig. 3). Judging from the result of yeast complementation test, AtAPG4 functions in autophagy in the same manner as yeast Apg4p, namely digest the extra amino acids tail downstream of the conserved Gly of AtAPG8 paralogs. Then, why AtAPG8h and AtAPG8i don't have an extra amino acids tail? Do these two molecules function in different biological process? In mammalian cells, there are three homologs of Apg8 and each mammalian Apg8 protein has been suggested to have additional functions other than autophagy (Wang et al.,

1999; Mann and Hammarback, 1994; Sagiv et al., 2000). Further characterization of each AtAPG8 molecule will hopefully yield the reason of this interesting gene duplication.

atapg9-1 is the first _APG_ gene knockout multicellular organism

Here, I succeeded to isolate the first plant knockout mutant of an autophagy-related gene. Recently, another group isolated an *AtAPG7* knockout plant, *atapg7-1*. Similar phenotypes to that of *atapg9-1*, such as starvation sensitivity and accelerated leaf senescence, were observed in *atapg7-1* (Doelling and Vierstra, personal communication). In addition to that while wild-type *AtAPG7* gene expression could rescue the phenotype of *atapg7-1*, the active site Cys mutant version of AtAPG7 could not, supporting that the molecular mechanisms involved in autophagy are well conserved among different organisms. AtAPG9 and AtAPG7 are the sole homolog of each yeast *APG* genes. The fact that common phenotypes were observed in *atapg9-1* and *atapg7-1* strongly supports the idea that their phenotypes are the result of defects in autophagy. However, the *atapg7-1* phenotype seems more severe than that of *atapg9-1* in several aspects. In mammalian cells, three homologs of yeast Apg8 were identified and human Apg7p activates all three of them and with human Apg12p (Tanida et al., 2001). As I mentioned before, each mammalian Apg8 protein has been suggested to have an additional function distinct from autophagy. Though interaction between AtAPG7 and all of the AtAPG8 proteins have not yet been demonstrated, the difference between the *atapg7-1* and *atapg9-1* phenotype will be explained after the biological function of each AtAPG8 protein is determined.

AtAPG9 is predicted as an integral membrane protein localized at cytosolic dot structure

To date, none of the structure related to autophagosome formation is known. Here, I found AtAPG9-GFP is localized to some cytosolic dot structures (Fig. 9). In yeast, the biochemical analysis indicates that Apg9p is an integral membrane protein and the immunofluorescence microscopic observation using HA-tagged Apg9p indicates Apg9p is localized to the punctate structures adjacent to the vacuole (Noda et al., 2000). Apg9p does not comigrate with typical endomembrane markers, trans Golgi network, vacuole, plasma membrane, ER and endosome, in sucrose density gradients and

immunoelectron microscopic analysis showed Apg9p localizes neither autophagic bodies nor autophagosomes. Taken together, Apg9p resides in perivacuolar punctate structures, which is largely distinct from known endomembrane compartments and possibly is the precursor structures of the autophagosome, and is required for functional localization of several Apg proteins (Wang et al., 2001; Noda et al., 2000; Suzuki et al., 2001). AtAPG9 was predicted to be an integral membrane protein, as is its homologue in yeast, and was expected to play an important role in autophagosome formation. These dot structures will be the similar compartments where Apg9p localizes in yeast. In such a case this is the first report on the structure related to autophagosome formation in plant cells. Recently, Suzuki et al. reported that Apg9p-GFP and GFP-Apg8p exist very near location occasionally (Suzuki et al., 2001). In onion epidermal cells, GFP-AtAPG8a also showed dot pattern dispersed in the cytosol (Yoshimoto, personal communication). However, the number of dot structures observed in cells expressing GFP-AtAPG8a is smaller than that of AtAPG9-GFP. It will be interesting to check if the same phenomenon is observed in plant cells and since plant cells are much lager than yeast and suitable for morphological research, that experiment may give us further information about AtAPG9 and AtAPG8 relation.

Spherical bodies observed under protease inhibitor treatment

The accumulation of spherical bodies by addition of cysteine protease inhibitor was reduced in *atapg9-1* root cells (Fig. 12). These spherical bodies observed in tobacco suspension-cultured cells are suggested as autolysosomes, which function as the degradation compartments in animal cell autophagy (Fig. 1). If these spherical bodies are autolysosomes, AtAPG9 must be involved in the sequestration process of substrate materials that are degraded inside of these spherical bodies. The defect in substrate transport process may cause the reduction in the number of these spherical bodies.

However, judging from the Figure 12, these spherical bodies exist inside of the vacuole. Thus, it is reasonable to consider these spherical bodies as autophagic bodies, not autolysosomes. In yeast, quinacrine stained autophagic bodies existing inside of the vacuole (Takeshige et al., 1992). I think that I observed the similar phenomenon in Arabidopsis root cells. In fact, in the case of sycamore cells and legume cotyledon cells, large central vacuoles are reported to function as the degradation compartment in autophagy. So in these cases, protease inhibitor treatment will cause the accumulation

of autophagic bodies inside the vacuole. There may be at least two macroautophagic pathways in plant cells, namely autolysosome involved pathway (like autophagy in animal cells) and vacuole involved pathway (like autophagy in yeast cells). The main macroautophagic pathway may be different according to the plant cell types or species. At least, under my experimental condition, Arabidopsis root cells seem to employ yeast-type macroautophagic pathway.

Then, if these spherical bodies are the autophagic bodies, shouldn't these spherical bodies were completely lost in *atapg9-1*? I think there will be other biological process to induce spherical bodies inside the vacuole without AtAPG9. As shown in Fig. 11A and B, even without protease inhibitor treatment, some spherical bodies were observed inside of the vacuole of Arabidopsis root cells. I didn't figure out what these structures really are so far, however, as these spherical bodies are stable structures, these structures seem to be different from autophagic bodies. Another possibility is that when function of AtAPG9 is lost, some autophagy-like activity still remain though most of them are abolished. Anyway, further characterization of these 'spherical bodies' are needed to describe the autophagy in plant cells in more detail.

Through the entire microscopic analysis of root cells, the significant defect in vacuole formation was not observed. This result indicates AtAPG9 is not involved in the vacuole biogenesis. As I mentioned before, functionally normal vacuole is formed in yeast *apg* mutants. Considering together, autophagy-like pathway observed during vacuole formation in plant cell will not depend on AtAPG molecules, there may be distinctive AtAPG-independent biological process that is morphologically alike AtAPG-dependent autophagic process.

atapg9-1 is sensitive to nutrient starvation

At early growth stages under nutrient conditions, a significant mutant phenotype was not observed in the *atapg9-1* mutant. However, nutrient starvation made it easy to distinguish *atapg9-1* from wild-type plants. *atapg9-1* plants began to die earlier than wild-type plants under both nitrogen and carbon starvation conditions (Fig. 13 and 15). Several preceding studies have indicated that autophagy is induced by nutrient starvation in other plant cells (Aubert et al., 1996; Moriyasu and Ohsumi, 1996). Here I described autophagic body like structure is induced by starvation. Therefore, the starvation-induced phenotype of *atapg9-1* must stem from a defect in autophagy.

Similar phenotypes were also observed in yeast (Tsukada and Ohsumi, 1993). During nitrogen starvation, wild-type yeast cells maintain viability, while *apg* mutant cells begin to die. The actual reason why autophagy-deficient yeast cells die is still unknown, though one possible explanation is that cytoplasmic constituents degraded by autophagy is meant to be utilized as a nutrient resource, which is necessary for maintaining cell viability during starvation. Alternatively, or additionally, yeast cell can not change themselves properly to starvation-resistant status without autophagic degradation. Anyway, autophagy seems to be important for resistance to starvation condition from yeast to plant.

Autophagy is regulated developmentally in addition to nutritional status

In yeast, autophagy is known to be triggered only by starvation. However, in addition to the starvation-induced phenotype, *atapg9-1* displayed early bolting and leaf senescence under nutrient conditions (Fig. 20 and 22). These results suggest that autophagy occurs in plants not only during starvation, but also under nutrient conditions. Indeed autophagy has been observed during natural leaf senescence (Inada et al., 1998; Minamikawa et al., 2001). Autophagy seems to be genetically programmed to occur during senescence regardless of nutrient status. In yeast, Tor protein kinase is the master regulator of autophagy. It senses nutrient condition, and when nutrient is rich, it regulates the cell to grow. When the nutrient is poor, it regulates the cell to induce autophagy (Noda et al., 1998). The similar mechanisms may underlie about plant autophagy. When nutrient is rich, the cell is regulated to proliferate. However, in a plant leaf, the proliferation is programmed to be finally stopped, and after several periods, they start to senesce naturally. Autophagy will be required during this transition, and the similar reciprocal regulation between growth and autophagy may exist in plant cells.

Autophagy and the efficient nutrient relocation

It is well known that plants relocate nutrients from old to young tissues. Nutrient relocation is an active process which must necessitate the integrity of plasmamembrane and the transporters. Early senescence and cell death must diminish the total amount of nutrient relocalized. Thus reduced seed sets (Fig. 14) in *atapg9-1* must be caused by the less efficient utilization of available nutrients in *atapg9-1*. In addition, here I

found that the timing of bolting was accelerated in *atapg9-1* under normal growth condition. The effect of nutrition on flowering time in Arabidopsis has not been analyzed in detail. In this research, I confirmed nitrogen status affects the flowering time in Arabidopsis, especially slight nitrogen starvation accelerates the flowering time (Fig. 21). Recently, effects of sugar on floral transition in Arabidopsis were investigated intensively (Ohto et al., 2001). In this study, addition of sugar in the medium retard the flowering time. These phenomenon are well explained as flowering is accelerated by poor nutrient environment. *atapg9-1* plant is possibly, in the slight nutrient-poor status. Although visible senescence does not occur at the time when bolting start, several rosette leaves had already expanded. As mentioned, autophagy must occur before senescence begins, these fully expanded leaves is possibly inducing autophagy. This kind of developmentally regulated autophagy may function in decreasing cellular activity by non selective degradation of house keeping protein, such as ribosome, and change the nature of the cell from proliferating status to quiescent status. The resulting degradation products may relocate to newly proliferating cells and affect the bolting time possibly at the meristem. More works of this type would be required to understand the effect of autophagy on the floral transition.

Autophagy does not play central role in degradation during leaf senescence

If autophagy contributes to the cellular degradation process during leaf senescence, then why is not the leaf senescence process inhibited in the *atapg9-1* plant, and why does it not remain green? Degradative processes other than autophagy are reported during senescence, such as degradation of chloroplast proteins by chloroplast intrinsic proteases (Bushnell et al., 1993) and the collapse of the vacuolar membrane (Inada et al., 1998). In addition, in the senescing soybean leaf, protrusion of numerous plastoglobules from chloroplasts was observed (Guiamet et al., 1999). These globules secreted from the chloroplast were suggested to carry the photosynthetic components to the cytoplasm or the vacuoles to be degraded. Park et al. reported a similar phenomenon, namely transfer of proteins from chloroplasts to vacuoles for degradation in *chlamydomonas reinhardtii* (Park et al., 1999). Leaf senescence in *atapg9-1* may depend on these other degradative processes.

The chlorophyll content of *atapg9-1* plant is apparently decreased more rapidly than that of wild-type. Ono et al. reported that two different phases of degradation occur in

wheat natural leaf senescence (Ono et al., 1995). About 20% of chloroplasts were lost during the first phase and the remainders were rapidly degraded during the second phase. In French bean leaves, 10% of chloroplasts were also degraded in the vacuole during artificially-induced senescence (Minamikawa et al., 2001). In the Arabidopsis mesophyll cells under artificially induced senescence, the same phenomenon, namely, reduction in the number of chloroplast may occurr. And the intensity of chlorophyll fluorescence in each chloroplast was also observed. In *atapg9-1* plant, both phenomenon proceeds and the decrease of number of chloroplast is also observed. More detailed quantitative analysis may be necessary to distinguish the small number of difference, however, at least, autophagy seems not to be mainly responsible for chloroplast degradation in this condition. On the contrary, both process proceed much faster than wild-type. At cellular level, it seemed different in the reduction rate of chloroplasts in the top region of mesophyll cells between wild-type and *atapg9-1* at 6 day (Fig. 19G and O). Besides, in each chloroplast level, the rate of chlorophyll loss was accelerated in *atapg9-1* (Fig. 19F and N).

How the AtAPG9 function cause differences in senescence? My current working model is shown in Figure. 23. Plant cells will orchestrate the regulation of several different degradation mechanisms during senescence to accomplish efficient nutrient relocation. Autophagy may help to maintain viability during senescence/starvation as seen in yeast, and even without autophagy, degradation process by mechanisms other than autophagy proceeds. However, the defect in autophagy induce the cell death in a earlier stage of senescence. Due to acceleration of cell death, *atapg9-1* may not be able to relocate nutrients efficiently, a process that requires ordered cell death dependent on autophagy.

This study provided the first hints as to when and where autophagy occurs in Arabidopsis. From the time course analysis of chlorophyll contents, *atapg9-1* plants start to show an aberrant phenotype at roughly day 3 after initiation of starvation. This suggests that autophagy was induced within 3 days after transfer, which is in agreement with results from studies on autophagy induction in cultured cells or in whole plants during starvation (Brouquisse et al., 1998; Moriyasu and Ohsumi, 1996). *AtAPG9* was expressed in all tested tissues, and thus autophagy may occur in all of these tissues. Due to its tendency to be degraded after isolation, however, biochemical studies on

AtAPG9 have not progressed thus far. Further study of this and other AtAPG proteins promises to yield a better understanding of autophagy in plants, both at the molecular and organismal level. Some of AtAPG proteins identified in this research are good candidates as the marker of autophagosome, they must provide powerful tool for further ultrastructural analysis of autophagy in Arabidopsis. How autophagy contributes to leaf senescence in Arabidopsis is also an interesting question to be investigated. This is the first report to describe the phenotype of an *APG* knockout multi-cellular organism. This is just the beginning of an exciting new stage in the study of plant autophagy.

References

Aubert S, Gout E, Bligny R, Marty-Mazars D, Barrieu F, Alabouvette J, Marty F, Douce R (1996) Ultrastructural and biochemical characterization of autophagy in higher plant cells subjected to carbon deprivation: control by the supply of mitochondria with respiratory substrates. J Cell Biol **133:** 1251-1263

Bhalla PL, Dalling MJ (1986) Endopeptidase and carboxypeptidase enzymes of vacuoles prepared from mesophyll protoplasts of the primary leaf of wheat seedling. J Plant Physiol **122:** 289-302

Brouquisse R, Gaudillere JP, Raymond P (1998) Induction of a carbon-starvation-related proteolysis in whole maize plants submitted to light/dark cycles and to extended darkness. Plant Physiol **117:** 1281-1291

Bushnell TP, Bushnell D, Jagendorf AT (1993) Purified zinc protease of pea chloroplasts, EP1, degrades the large subunit of ribulose-1,5-bisphosphate carboxylase/oxygenase. Plant Physiol **103:** 585-591

Chen MH, Liu LF, Chen YR, Wu HK, Yu SM (1994) Expression of alpha-amylases, carbohydrate metabolism, and autophagy in cultured rice cells is coordinately regulated by sugar nutrient. Plant J **6:** 625-636

Clough SJ, Bent AF (1998) Floral dip: a simplified method for *Agrobacterium*-mediated transformation of *Arabidopsis thaliana*. Plant J **16:** 735-743

Cutler SR, Ehrhardt DW, Griffitts JS, Somerville CR (2000) Random GFP::cDNA fusions enable visualization of subcellular structures in cells of Arabidopsis at a high frequency. PNAS **97:** 3718-3723

DunnWA (1990a) Studies on the mechanisms of autophagy: formation of the autophagic vacuole. J Cell Biol 110: 1923-1933

DunnWA (1990b) Studies on the mechanisms of autophagy: maturation of the autophagic vacuole. J Cell Biol 110: 1935-1945

Funakoshi T, Matsuura A, Noda T, Ohsumi Y (1997) Analyses of *APG13* gene involved in autophagy in yeast, *Saccharomyces cerevisiae*. Gene **192:** 207-213

Genix P, Bligny R, Martin JB, Douce R (1990) Transient accumulation of asparagines in sycamore cells after a long period of sucrose starvation. Plant Physiol. **94:** 717-22

Guiamet JJ, Pichersky E, Nooden LD (1999) Mass exodus from senescing soybean chloroplasts. Plant Cell Physiol **40:** 986-992

Hayashi M, Nito K, Toriyama-Kato K, Kondo M, Yamaya T, Nishimura M (2000) *At*Pex14p maintains peroxisomal functions by determining protein targeting to three kinds of plant peroxisomes. EMBO J **19:** 5701-5710

Hirai MY, Fujiwara T, Chino M, Naito S (1995) Effects of sulfate concentrations on the expression of a soybean seed storage protein gene and its reversibility in transgenic *Arabidopsis thaliana*. Plant Cell Physiol **36:** 1331-1339

Ichimura Y, Kirisako T, Takao T, Satomi Y, Shimonishi Y, Ishihara N, Mizushima N, Tanida I, Kominami E, Ohsumi M, Noda T, Ohsumi Y (2000) A ubiquitin-like system mediates protein lipidation. Nature **408:** 488-492

Inada N, Sakai A, Kuroiwa H, Kuroiwa T (1998) Three-dimensional analysis of the senescence program in rice (*Oryza sativa L.*) coleoptiles: investigations by fluorescence microscopy and electron microscopy. Planta **206:** 585-597

Ishida H, Nishimori Y, Sugisawa M, Makino A, Mae T (1997) The large subunit of ribulose-1, 5-bisphosphate carboxylase/oxygenase is fragmented into 37-kDa and 16-kDa polypeptides by active oxygen in the lysates of chlorplasts from primary leaves of wheat. Plant Cell Physiol **38:** 471-479

Kabeya Y, Mizushima N, Ueno T, Yamamoto A, Kirisako T, Noda T, Kominami E, Ohsumi Y, Yoshimori T (2000) LC3, a mammalian homologue of yeast Apg8p, is localized in autophagosome membrane after processing. EMBO J **19:** 5720-5728

Kamada Y, Funakoshi T, Shintani T, Nagano K, Ohsumi M, Ohsumi Y (2000) Tor-mediated induction of autophagy via an Apg1 protein kinase complex. J Cell Biol **150:** 1507-1513

Kirisako T, Ichimura Y, Okada H, Kabeya Y, Mizushima N, Yoshimori T, Ohsumi M, Noda T, Ohsumi Y (2000) Reversible modification regulares the memrane-binding state of Apg8/Aut7 essential for autophagy and the cytoplasm to vacuole targeting pathway. J Cell Biol **151:** 263-276

Klionsky DJ, Ohsumi Y (1999) Vacuolar import of proteins and organelles from the cytoplasm. Annu Rev Cell Dev Biol **15:** 1-32

Kyte J. Doolittle RF (1982) A simple method for displaying the hydropathic character of protein. J Mol Biol **157:** 105-132

Liang XH, Jackson S, Seaman M, Brown K, Kempkes B, Hibshoosh H, Levine B (1999) Induction of autophagy and inhibition of tumorigenesis by *beclin 1*. Nature **402:** 672-676

Lin W, Wittenbach VA (1981) Subcellular localization of proteases in wheat and corn mesophyll protoplasts. Plant Physiol **67:** 969-972

Liu XQ, Jagendorf AT (1984) ATP-dependent proteolysis in pea chloroplasts. FEBS Lett **166**: 248-252

Mae T, Kai N, Makino A, Ohira K (1984) Relation between ribulose bisphosphate carboxylase content and chloroplast number in naturally senescing primary leaves of wheat. Plant Cell Physiol **25:** 333-336

Mae T, Kamei C, Funaki K, Miyadai K, Makino A, Ohira K, Ojima K (1989) Degradation of ribulose-1, 5-bisphosphate carboxylase/oxygenase in the lysates of the chloroplasts isolated mechanically from wheat (Triticum aestivum L.) leaves. Plant Cell Physiol **30:** 193-200

Mann SS, Hammarback JA (1994) Molecular characterization of light chain 3. A microtubule binding subunit of MAP1A and MAP1B. J Biol Chem **269:** 11492-114497

Marty F (1978) Cytochemical studies on GERL, provacuoles, and vacuoles in root meristematic cells of *Euphorbia*. Proc Natl Acad Sci USA **75:** 852-856

Marty F (1999) Plant vacuoles. Plant Cell **11:** 587-599

Matile P, Winkenbach F (1971) Function of lysosomes and lysosomal enzymes in the senescing corolla of the morning glory. J Exp Bot **22:** 759-771

Matile P (1975) The lytic compatment of plant cells. *In* Cell Biology Monographs, Vol. 1. Springer-Verlag, Wien, Germany

Matile P (1997) The vacuole and cell senescence. Adv Bot Res **25**: 87-112

Matsuura A, Tsukada M, Wada Y, Ohsumi Y (1997) Apg1p, a novel protein kinase required for the autophagic process in *Saccharomyces cerevisiae*. Gene **192:** 245-250

McKinney EC, Ali N, Traut A, Feldmann KA, Belostotsky DA, McDowell JM, Meagher RB (1995) Sequence-based identification of T-DNA insertion mutations in *Arabidopsis*: actin mutants *act2-1* and *act4-1*. Plant J. **8:** 613-622

Minamikawa T, Toyooka K, Okamoto T, Hara-Nishimura I, Nishimura M (2001) Degradation of ribulose 1,5-biphosphate carboxylase/oxygenase by vacuolar enzymes of senescing french bean leaves: immunocytochemical and ultrastructural observations. Protoplasma in press

Miyadai K, Mae T, Makino A, Ojima K (1990) Characteristics of Ribulose-1, 5-bisphosphate carboxylase/oxygenase degradation by lysates of mechanically isolated chloroplasts from wheat leave. Plant Physiol **92:** 1215-1219

Mizushima N, Noda T, Yoshimori T, Tanaka Y, Ishii T, George MD, Klionsky DJ, Ohsumi M, Ohsumi Y (1998a) A protein conjugation system essential for autophagy. Nature **395:** 395-398

Mizushima N, Sugita H, Yoshimori T, Ohsumi Y (1998b) A new protein conjugation system in human. The counterpart of the yeast Apg12p conjugation system essential for autophagy. J Biol Chem **273:** 33889-33892

Mizushima N, Yamamoto A, Hatano M, Kobayashi Y, Kabeya Y, Suzuki K, Tokuhisa T, Ohsumi Y, Yoshimori T (2001) Dissection of autophagosome formation using Apg5-deficient mouse embryonic stem cells. J Cell Biol **152:** 657-667

Moran R (1982) Formulae for determination of chlorophyllous pigments extracted with N, N-dimethylformamide. Plant Physiol **69:** 1376-1381

Moriyasu Y, Hillmer S (2000) Autophagy and vacuole formation. *In* Robinson DG, Rogers JC, eds, Vacuolar compartments. Annu Plant Rev **5:** 71-89

Moriyasu Y, Ohsumi Y (1996) Autophagy in tobacco suspension-cultured cells in response to sucrose starvation. Plant Physiol **111:** 1233-1241

Musgrove JE, Elderfield PD, Robinson C (1989) Endopeptidases in the stroma and thylakoids of pea chloroplasts. Plant Physiol **90:** 1616-1621

Noda T, Ohsumi Y (1998) Tor, a phosphatidylinositol kinase homologue, controls autophagy in yeast. J Biol Chem **273:** 3963-6

Noda T, Kim J, Huang WP, Baba M, Tokunaga T, Ohsumi Y, Klionsky DJ (2000) Apg9p/Cvt7p is an integral membrane protein required for transport vesicle formation in the cvt and autophagy pathways. J Cell Biol **148:** 465-479

Oh SA, Lee SY, Chung IK, Lee CH, Nam HG (1996) A senescence-associated gene of *Arabidopsis thaliana* is distinctively regulated during natural and artificially induced leaf senescence. Plan Mol Biol **30:** 739-754

Ohsumi Y (2001) Molecular dissection of autophagy. Two ubiquitin-like systems. Nature Rev Mol Cell Biol **2:** 211-216

Ohto M, Onai K, Furukawa Y, Aoki E, Araki T, Nakamura K (2001) Effects of sugar on vegetative development and floral transition in arabidopsis. Plant Physiol **127:** 252-261

Ono K, Hashimoto H, Katoh S (1995) Changes in the number and size of chloroplasts during senescence of primary leaves of wheat grown under different conditions. Plant Cell Physiol **36:** 9-17

Park H, Eggink LL, Roberson RW, Hoober JK (1999) Transfer of proteins from the chloroplast to vacuoles in *chlamydomonas reinhardtii* (chlorophyta): A pathway for degradation. J Phycol **35:** 528-538

Rojo E, Gillmor CS, Kovaleva V, Somerville CR, Raikhel NV (2001) *VACUOLESS1* is an essential gene required for vacuole formation and morphogenesis in Arabidopsis Dev Cell **1:** 303-310

Sakai Y, Koller A, Rangell LK, Keller GA, Subramani S (1998) Peroxisome degradation by microautophagy in Pichia pastoris: Identification of specific steps and morphological intermediates. J Cell Biol **141:** 625-636

Sagiv Y, Legesse-Miller A, Porat A, Elazar Z (2000) GATE-16, a membrane transport modulator, interacts with NSF and the Golgi v-SNARE GOS-28. EMBO J **19:** 1494-1504

Shanklin J, De Witt ND, Flanagan JM (1995) The stroma of plant plastids contain ClpP and ClpC, functional homolog of Escherichia coli ClpP and ClpA; an archetypal two-component ATP-dependent protease. Plant Cell **7:** 1713-1722

Shintani T, Mizushima N, Ogawa Y, Matsuura A, Noda T, Ohsumi Y (1999) Apg10p, a novel protein-conjugating enzyme essential for autophagy in yeast. EMBO J **18:** 5234-5241

Suzuki K, Kirisako T, Kamada Y, Mizushima N, Noda T, Ohsumi Y (2001) The pre-autophagosomal structure organized by concerted functions of *APG* genes is essential for autophagosome formation. EMBO J in press

Takeshige K, Baba M, Tsuboi S, Noda T, Ohsumi Y (1992) Autophagy in yeast demonstrated with proteinase-deficient mutants and conditions for its induction. J Cell Biol **119:** 301-311

Tanaka K, Nakafuku M, Tamanoi F, Kaziro Y, Matsumoto K, Toh-e A (1990) IRA2, a second gene of *Saccharomyces cerevisiae* that encodes a protein with a domain homologous to mammalian ras GTPase-activating protein. Mol Cell Biol **10:** 4303-4313

Tanida I, Mizushima N, Kiyooka M, Ohsumi M, Ueno T, Ohsumi Y, Kominami E (1999) Apg7p/Cvt2p: A novel protein-activating enzyme essential for autophagy. Mol Biol Cell **10:** 1367-1379

Tanida I, Tanida-Miyake E, Ueno T, Kominami E (2001) The human homolog *of Saccharomyces cerevisiae* Apg7p is a protein-activating enzyme for multiple substrates including human Apg12p, GATE-16, GABARAP, and MAP-LC3. J Biol Chem **276:**

1701-1706

Thayer SS, Huffaker RC (1984) Vacuolar localization of endoproteinases EP1 and EP2 in barley mesophyll cells. Plant Physiol **75:** 70-73

Thomas H, Huffaker RC (1981) Hydrolysis of radioactively-labelled

Thumm M, Egner R, Koch B, Schlumpberger M, Straub M, Veenhuis M, Wolf DH (1994) Isolation of autophagocytosis mutants of *Saccharomyces cerevisiae*. FEBS Lett **349:** 275-280

Toyooka K, Okamoto T, Minamikawa T (2001) Cotyledon cells of *Vigna mungo* seedlings utilize at least two distinct autophagic machineries for degradation of starch granules and cellular components. J Cell Biol **154:** 973-982

Tsukada M, Ohsumi Y (1993) Isolation and characterization of autophagy-defective mutants of *Saccharomyces cerevisiae*. FEBS Lett **333:** 169-174

Van der Wilden W, Herman EM, Chrispeels MJ (1990) Protein bodies of mung bean cotyledons as autophagic organelles. Proc Natl Acad Sci USA **77:** 428-432

Vierstra RD (1996) Proteolysis in plants: mechanisms and functions. Plant Molecular Biology **32:** 275-302

Wang CW, Kim J, Huang WP, Abeliovich H, Stromhaug PE, Dunn WA, Klionsky DJ (2001) Apg2 is a novel protein required for the cytoplasm to vacuole targeting, autophagy, and pexophagy pathways. J Biol Chem **276:** 30442-30451

Wang H, Bedford FK, Brandon NJ, Moss SJ, Olsen RW (1999) $GABA_A$-receptor-associated protein links $GABA_A$ receptors and the cytoskeleton. Nature **397:** 69-72

Waters SP, Noble ER, Dalling MJ (1982) Intercellular localization of peptide hydrolases in wheat (*Triticum aestivum* L.) leaves. Plant Physiol **69:** 575-579

Wardley TM, Bhalla PL, Dalling MJ (1984) Changes in the number and composition of chloroplasts during senescence of mesophyll cells of attached and detached primary leaves of wheat (*Triticum aestivum* L.). Plant Physiol **75:** 421-424

Wittenbach VA, Lin W, Habert RR (1982) Vacuolar localization of proteases and degradation of chloroplasts in mesophyll protoplasts from senescing primary wheat leaves. Plant Physiol **69:** 98-102

Yoshida T, Minamikawa T (1996) Successive amino-terminal proteolysis of the large subunit of ribulose 1,5-bisphosphate carboxylase/oxygenase by vacuolar enzymes from French bean leaves. FEBS Lett **238:** 317-324